arXiv:2009.05732v2 [q-bio.PE] 10 Nov 2020

The challenges of containing SARS-CoV-2 via test-trace-and-isolate

Sebastian Contreras[1, 2, X], **Jonas Dehning**[1, X], **Matthias Loidolt**[1, X], **Johannes Zierenberg**[1], **F. Paul Spitzner**[1], **Jorge H. Urrea-Quintero**[1], **Sebastian B. Mohr**[1], **Michael Wilczek**[1,3], **Michael Wibral**[4], **and Viola Priesemann**[1,3*]

[1]Max Planck Institute for Dynamics and Self-Organization, Am Faßberg 17, 37077 Göttingen, Germany.
[2]Centre for Biotechnology and Bioengineering, Universidad de Chile, Beauchef 851, 8370456 Santiago, Chile.
[3]Institute for the Dynamics of Complex Systems, University of Göttingen, Friedrich-Hund-Platz 1, 37077 Göttingen, Germany.
[4]Campus Institute for Dynamics of Biological Networks, University of Göttingen, Hermann-Rein-Straße 3, 37075 Göttingen, Germany.
[X]These authors contributed equally: Sebastian Contreras, Jonas Dehning, Matthias Loidolt

Abstract

Without a cure, vaccine, or proven long-term immunity against SARS-CoV-2, test-trace-and-isolate (TTI) strategies present a promising tool to contain its spread. For any TTI strategy, however, mitigation is challenged by pre- and asymptomatic transmission, TTI-avoiders, and undetected spreaders, who strongly contribute to "hidden" infection chains. Here, we studied a semi-analytical model and identified two tipping points between controlled and uncontrolled spread: (1) the behavior-driven reproduction number R_t^H of the hidden chains becomes too large to be compensated by the TTI capabilities, and (2) the number of new infections exceeds the tracing capacity. Both trigger a self-accelerating spread. We investigated how these tipping points depend on challenges like limited cooperation, missing contacts, and imperfect isolation. Our model results suggest that TTI alone is insufficient to contain an otherwise unhindered spread of SARS-CoV-2, implying that complementary measures like social distancing and improved hygiene remain necessary.

***K*eywords** COVID-19 · SARS-CoV-2 · Contact tracing · Test-Trace-Isolate TTI · Test-Trace-Isolate-Support · Containment strategies · Mitigation · Asymptomatic transmission · epidemiology · SIR model

Introduction

After SARS-CoV-2 started spreading rapidly around the globe in early 2020, many countries have successfully curbed the initial exponential rise in case numbers ("first wave"). Most of the successful countries employed a mix of measures combining hygiene regulations and mandatory physical distancing to reduce the reproduction number and the number of new infections [1, 2] together with testing, contact tracing, and isolation (TTI) of known cases [3, 4]. Among these measures, those aimed at distancing — like school closures and a ban of all unnecessary social contacts ("strict lockdown") — were highly controversial, but have proven effective [1, 2]. Notwithstanding, distancing measures put an enormous burden on society and economy. In countries that have controlled the initial outbreak, there is a strong motivation to relax distancing measures, albeit under the constraint to keep the spread of COVID-19 under control [5, 6].

In principle, it seems possible that both goals can be reached when relying on the increased testing capacity for SARS-CoV-2 infections if complemented by contact tracing and quarantine measures (e.g. like TTI

*viola.priesemann@ds.mpg.de

strategies [4]); South Korea and Singapore illustrate the success of such a strategy [7–9]. In practice, resources for testing are still limited and costly, and health systems have capacity limits for the number of contacts that can be traced and isolated; these resources have to be allocated wisely in order to control disease spread [10].

TTI strategies have to overcome several challenges to be effective. Infected individuals can become infectious before developing symptoms [11, 12], and because the virus is quite infectious, it is crucial to minimize testing and tracing delays [13]. Furthermore, SARS-CoV-2 infections generally appear throughout the whole population (not only in regional clusters), which hinders an efficient and quick implementation of TTI strategies.

Hence, these challenges that impact and potentially limit the effectiveness of TTI need to be incorporated together into one model of COVID-19 control, namely (1) the existence of asymptomatic, yet infectious carriers [14, 15] — which are a challenge for symptom-driven but not for random testing strategies; (2) the existence of a certain fraction of the population that is opposed to taking a test, even if symptomatic [16]; (3) the capacity limits of contact tracing and additional imperfections due to imperfect memory or non-cooperation of the infected. Last, enormous efforts are required to completely prevent influx of COVID-19 cases into a given community, especially during the current global pandemic situation combined with relaxed travel restrictions [5, 17]. This influx makes virus eradication impossible; it only leaves a stable level of new infections or their uncontrolled growth as the two possible regimes of disease dynamics. Thus, policy makers at all levels, from nations to federal states, all the way down to small units like enterprises, universities or schools, are faced with the question of how to relax physical distancing measures while confining COVID-19 progression with the available testing and contact-tracing capacity [18].

Here, we employ a compartmental model of SARS-CoV-2 spreading dynamics that incorporates the challenges (1)-(3). We base the model parameters on literature or reports using the example of Germany. The aim is to determine the critical value for the reproduction number in the general (not quarantined) population (R^H_{crit}), for which disease spread can still be contained. We find that — even under an optimal use of the available testing and contract tracing capacity — the *hidden* reproduction number R^H_t has to be maintained at sufficiently low levels, namely $R^H_t < R^H_{\text{crit}} \approx 2$ (95 % CI: 1.42–2.70). Hence, hygiene and physical distancing measures are required in addition to TTI to keep the virus spread under control. To further assist the efficient use of resources, we investigate the relative merits of contact tracing, symptom-driven and random testing. We demonstrate the danger of a tipping point associated to the limited capacity of tracing contacts of infected people. Last but not least, we show how either testing scheme has to be increased to re-stabilize disease spread after an increase in the reproduction number.

Results

Model Overview

We developed an SIR-type model [19, 20] with multiple compartments that incorporates the effects of test-trace-and-isolate (TTI) strategies (for a graphical representation of the model see Fig. 1 and Supplementary Fig. 1). We explore how TTI can contain the spread of SARS-CoV-2 for realistic scenarios based on the TTI system in Germany. A major difficulty in controlling the spread of SARS-CoV-2 are the cases that remain hidden and behave as the general population does, potentially having many contacts. We explicitly incorporate such a "hidden" pool H into our model and characterize the spread within by the reproduction number R^H_t, which reflects the population's contact behavior. Cases remain hidden until they enter a "traced" pool through testing or by contact tracing of an individual that has already been tested positive (see Fig. 1). All individuals in the traced pool T isolate themselves (quarantine), reducing the reproduction number to R^T_t. Apart from a small leak, novel infections therein are then assumed to remain within the traced pool. We investigate both symptom-driven and random testing, which differ in the cases they can reveal: random testing can in principle uncover even asymptomatic cases, while symptom-driven testing is limited to symptomatic cases willing to be tested. Parameters describing the spreading dynamics (Tab. 1) are based on the available literature on COVID-19 [1, 15, 16, 22, 23], while parameters describing the TTI system are inspired by our example case Germany wherever possible.

We provide the code of the different analyses at `https://github.com/Priesemann-Group/covid19_tti`. An interactive platform to simulate scenarios different from those presented here is available (beta-version) on the same GitHub repository.

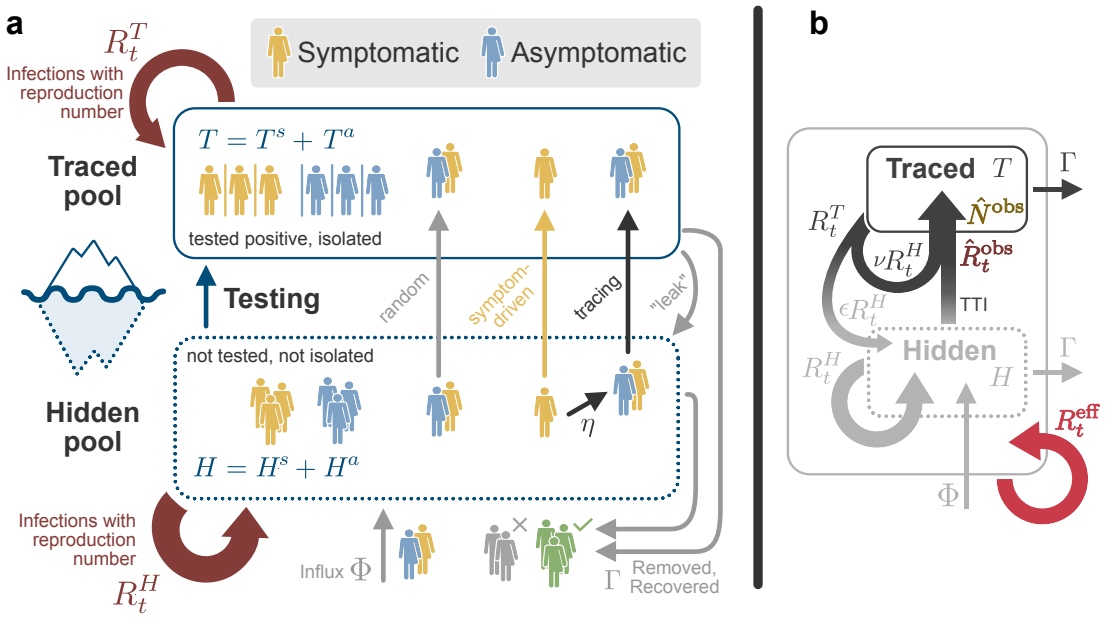


Figure 1: **Illustration of interactions between the hidden H and traced T pools in our model. (a)** In our model, we distinguish two different infected population groups: the one that contains the infected individuals that remain undetected until tested (hidden pool H), and the one with infected individuals that we already follow and isolate (traced pool T). Until noticed, an outbreak will fully occur in the hidden pool, where case numbers increase according to this pool's reproduction number R_t^H. Testing and tracing of hidden infections transfers them to the traced pool and helps to empty the hidden pool; this prevents offspring infections and reduces the overall growth of the outbreak. Due to the self-isolation imposed in the traced pool, its reproduction number R_t^T is expected to be considerably smaller than R_t^H, and typically smaller than 1. Once an individual is tested positive, all the contacts since the infection are traced with some efficiency (η). Two external events further increase the number of infections in the hidden pool, namely, the new contagions occurring in the traced pool that leak to the hidden pool (ϵ) and an influx of externally acquired infections (Φ). In the absence of new infections, pool sizes are naturally reduced due to recovery (or removal), proportional to the recovery rate Γ. **(b)** Simplified depiction of the model showing the interactions of the two pools. Note that the central epidemiological observables are highlighted in colour: The $\hat{N}^{\text{obs}}$ (brown) and $\hat{R}_t^{\text{obs}}$ (dark red) can be inferred from the traced pool, but the effective reproduction number $\hat{R}_t^{\text{eff}}$ (light red) that governs the stability of the whole system remains hidden.

TTI strategies can in principle control SARS-CoV-2 spread

To demonstrate that TTI strategies can in principle control the disease spread, we simulated a new outbreak starting in the hidden pool (Fig. 2). We assume that the outbreak is unnoticed initially, and then evaluate the effects of two alternative testing and contact tracing strategies starting at day 0: Contact tracing is either efficient, i.e. 66% ($\eta = 0.66$) of the contacts of a positively tested person are traced and isolated without delay ("efficient tracing"), or contact tracing is assumed to be less efficient, identifying only 33% of the contacts ("inefficient tracing"). In both regimes, the default parameters are used (Tab. 1), which include symptom-driven testing with rate $\lambda_s = 0.1$, and isolation of all tested positively, which reduces their reproduction number by a factor of $\nu = 0.1$.

Efficient contact tracing rapidly depletes the hidden pool H and populates the traced pool T, and thus stabilizes the total number of infections $T + H$ (Fig. 2a). The system relaxes to its equilibrium, which is a function of TTI and epidemiological parameters (Supplementary Equations (3)–(5)). Consequently, the observed number of daily infections ($\hat{N}^{\text{obs}}$) approaches a constant value (Fig. 2b), while the observed reproduction number $\hat{R}_t^{\text{obs}}$ approaches unity (Fig. 2c), further showing that effective TTI can be sufficient to stabilize the disease spread with $R_t^H = 1.8$.

In contrast, inefficient contact tracing cannot deplete the hidden pool sufficiently quickly to stabilize the total number of infections (Fig. 2d). Thus, the absolute and the observed daily number of infections N continue to grow approximately exponentially (Fig. 2e). In this case, the TTI strategy with ineffective contact tracing slows the spread, but cannot control the outbreak.

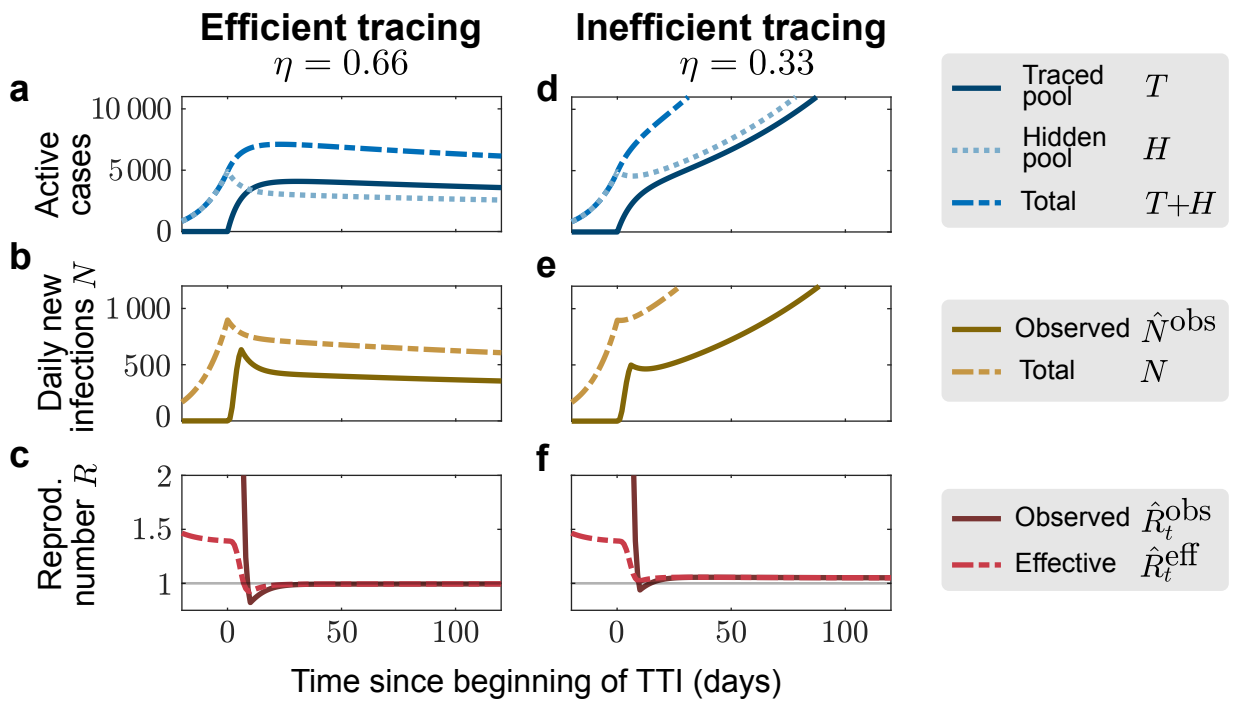


Figure 2: **Sufficient testing and contact tracing can control the disease spread, insufficient TTI only slows it.** We consider a TTI strategy with symptom-driven testing ($\lambda_s = 0.1$) and two tracing scenarios: For high tracing efficiency ($\eta = 0.66$, **(a-c)**), the outbreak can be controlled by TTI; for low tracing efficiency ($\eta = 0.33$, **(d-e)**) the outbreak cannot be controlled because tracing is not efficient enough. **(a,d)** The number of infections in the hidden pool grows until the outbreak is noticed on day 0, at which point symptom-driven testing ($\lambda_s = 0.1$) and contact tracing (η) starts. **(b,e)** The absolute number of daily infections (N) grows until the outbreak is noticed on day 0; the observed number of daily infections ($\hat{N}^{\mathrm{obs}}$) shown here is simulated as being inferred from the traced pool and subject to a gamma-distributed reporting delay with a median of 4 days. **(c,f)** The observed reproduction number $\hat{R}_t^{\mathrm{obs}}$ is estimated from the observed new infections $\hat{N}^{\mathrm{obs}}$. After an initial growth period, it settles to $\hat{R}_t^{\mathrm{obs}} = 1$ if the outbreak is controlled (efficient tracing), or to $\hat{R}_t^{\mathrm{obs}} > 1$ if the outbreak continues to spread (inefficient tracing). All the curves plotted are obtained from numerical integration of equations (1) - (5).

TTI extends the stabilized regimes of spreading dynamics

Comparing the two TTI strategies from above demonstrates that two distinct regimes of spreading dynamics are attainable under the condition of a non-zero influx of externally acquired infections Φ: The system either evolves towards some intermediate, but stable number of new cases N (Fig. 2a-c), or it is unstable, showing a steep growth (Fig. 2d-f). These two dynamical regimes are characterized — after an initial transient — by different "observed" reproduction numbers $\hat{R}_t^{\mathrm{obs}}$, inferred from the new cases of the traced pool $\hat{N}^{\mathrm{obs}}$. If $\hat{R}_t^{\mathrm{obs}} < 1$, the outbreak is under control (solid line in Fig. 2c), while for $\hat{R}_t^{\mathrm{obs}} > 1$ the outbreak continues to spread (Fig. 2f). The former regime extends the "stable" regime of the simple SIR model beyond $R_t^H = 1$ and thus constitutes a novel "TTI-stabilized" regime of spreading dynamics (Fig. 5, see Supplementary Fig. 5 for the full phase diagram).

Limited tracing capacity requires a safety margin to maintain stability

Having demonstrated that an effective TTI strategy can in principle control the disease spread, we now turn towards the problem of limited TTI capacity. So far, we assumed that the efficiency of the TTI strategy does not depend on the absolute number of cases. Yet, the amount of contacts that can reliably be traced by health authorities is limited due to the work to be performed by trained personnel: Contact persons have to be identified, informed, and ideally also counseled during the preventive quarantine. Exceeding this limit causes delays in the process, which will eventually become longer than the generation time of 4 days -

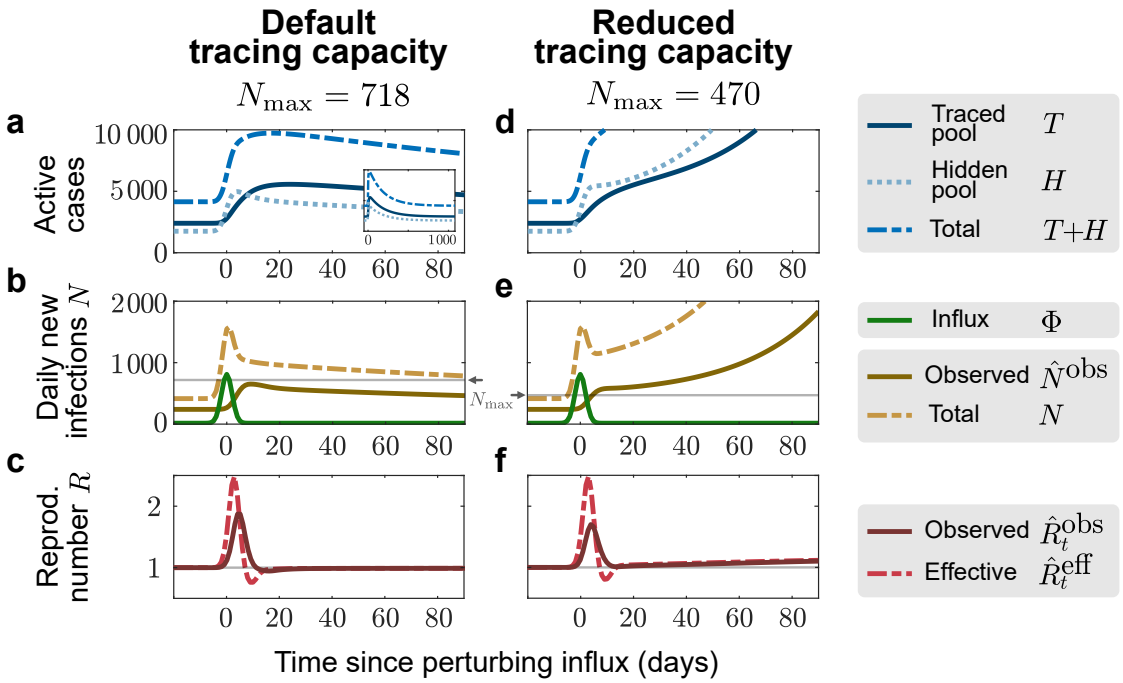


Figure 3: **Finite tracing capacity makes the system vulnerable to large influx events.** A single large influx event (a total of 4000 hidden cases with 92% occurring in the 7 days around $t = 0$, normally distributed with $\sigma = 2$ days) drives a meta-stable system with reduced tracing capacity (reached at $N_{\max} = 470$) to a new outbreak **(d-f)**, whereas a meta-stable system with our default tracing capacity (reached at $N_{\max} = 718$) can compensate a sudden influx of this size **(a-c)**. **(a,d)** The number of infections in the hidden pool (dotted) jump due to the influx event at $t = 0$, and return to stability for default capacity (a) or continue to grow in the system with reduced capacity (d). Correspondingly, the number of cases in the traced pool (solid line) either slowly increases after the event, and absorbs most infections before returning to stability (inset in A, time axis prolonged to 1000 days), or proceeds to grow steeply (d). **(b,e)** The absolute number of new infections (dashed, yellow) jumps due to the large influx event (solid green line). The number of daily observed cases (solid brown line) slowly increases after the event, and relaxes back to baseline (a), or increases fast upon exceeding the maximum number of new observed cases $N_{\max}$ (solid grey line) for which tracing is effective. **(c,f)** The effective (dashed red line) and observed (solid dark red line) reproduction numbers change transiently due to the influx event, before returning to 1 for the default tracing capacity. In the case of a reduced tracing capacity and a new outbreak, they slowly begin to grow afterwards (f). All the curves plotted are obtained from numerical integration of equations (1) - (5).

rendering contact tracing ineffective. We model this tracing capacity as a hard cap N_{max} on the amount of contacts that can be traced each day and explore its effects on stability.

As an example of how this limited tracing capacity can cause a new tipping point to instability, we simulate here a short but large influx of externally acquired infections (a total of 4000 hidden cases with 92% occurring in the 7 days around $t = 0$, normally distributed with $\sigma = 2$ days, see Fig. 3). This exemplary influx is inspired from the large number of German holidaymakers returning from summer vacation, and is a rather conservative estimate given that there were 900 such cases observed in the first two weeks of July at Bavarian highway test-centres alone [24]. We set two different tracing-capacity limits, reached when the observed number of daily new cases $\hat{N}^{\text{obs}}$ reaches $N_{\max} = 718$ (or $N_{\max} = 470$) observed cases per day (see methods). In both scenarios, the sudden influx leads to a jump of infections in the hidden pool (Fig. 3a,d), followed by a fast increase in new traced cases (Fig. 3b,e). With sufficiently high tracing capacity, the outbreak can then be contained, because during the initial shock $\hat{N}^{\text{obs}}$ does not exceed the capacity limit $N_{\max}$ (Fig. 3b, brown vs grey lines). In contrast, with lower capacity, the outbreak accelerates as soon as the observed new cases $\hat{N}^{\text{obs}}$ exceeds the capacity limit $N_{\max}$. Not only the capacity limit, but also the amplitude of the influx (Supplementary Fig. 3), its duration (Supplementary Fig. 4) or whether it occurs periodically (Fig. 4) can decide whether the observed new cases $\hat{N}^{\text{obs}}$ exceed the capacity limit $N_{\max}$ and cause a tipping-over into instability. In particular, periodic influxes (e.g. holidays) may cause the tipping-over not necessarily because of a single event but due to their cumulative impact. These scenarios demonstrate that the limited tracing

capacity renders the system meta-stable: if the capacity limit is exceeded due to some external perturbation, the tracing cannot compensate the perturbation and the spread gets out of control.

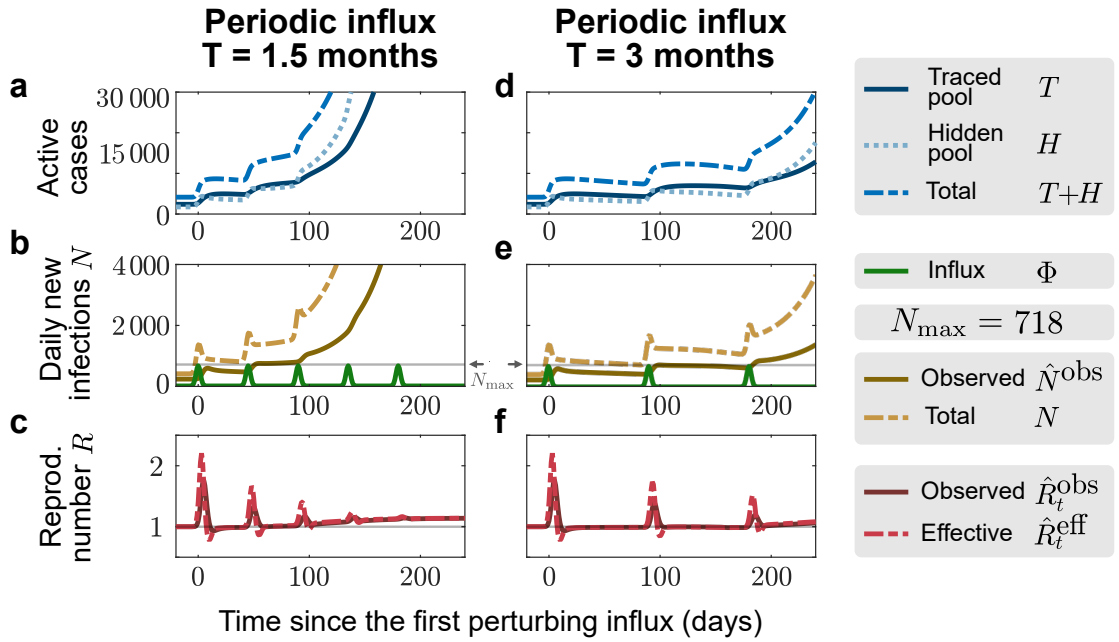


Figure 4: **Manageable influx events that recur periodically can overwhelm the tracing capacity.** For the default capacity scenario, we explore whether periodic influx events can overwhelm the tracing capacity: A "manageable" influx that would not overwhelm the tracing capacity on its own (3331 externally acquired infections, 92% of which occur in 7 days) repeats every 1.5 months **(a-c)** or every 3 months **(d-f)**. In the first case, the system is already unstable after the second event because case-numbers remained high after the first influx **(b)**. In the second case, the system remains stable after both the first and second event **(e)**, but it becomes unstable after the third **(f)**.

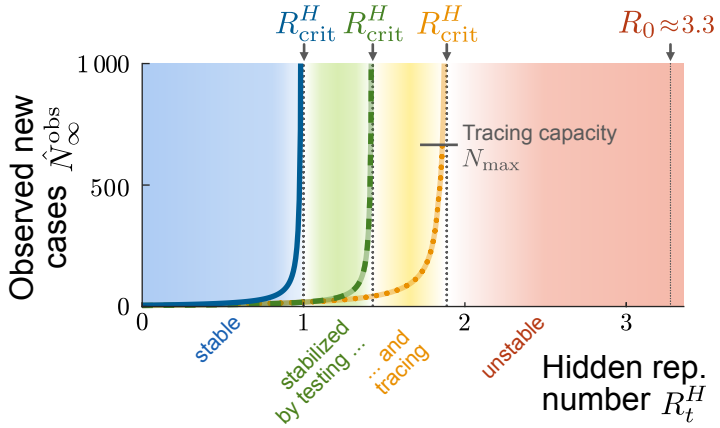


Figure 5: **Testing and tracing give rise to two TTI-stabilized regimes of spreading dynamics.** In addition to the intrinsically stable regime of the simple SIR model (blue region), our model exhibits two TTI-stabilized regimes that arise from the isolation of formerly "hidden" infected individuals uncovered through symptom-based testing alone (green region) or additional contact-tracing (amber region). Due to the external influx, the number of observed new cases reaches a non-zero equilibrium $\hat{N}^{\text{obs}}_{\infty}$ that depends on the hidden reproductive number (coloured lines). These equilibrium numbers of new cases diverge when approaching the respective critical hidden reproductive numbers calculated from linear stability analysis (dotted horizontal lines). Taking into account a finite tracing capacity $N_{\max}$ shrinks the testing-and-tracing stabilized regime and makes it meta-stable (dotted amber line). Note that, for our standard parameter set, the natural base reproduction number R_0 lies in the unstable regime. Please see Fig. 5 for a full phase diagram and Supplementary Section 2 for the linear stability analysis.

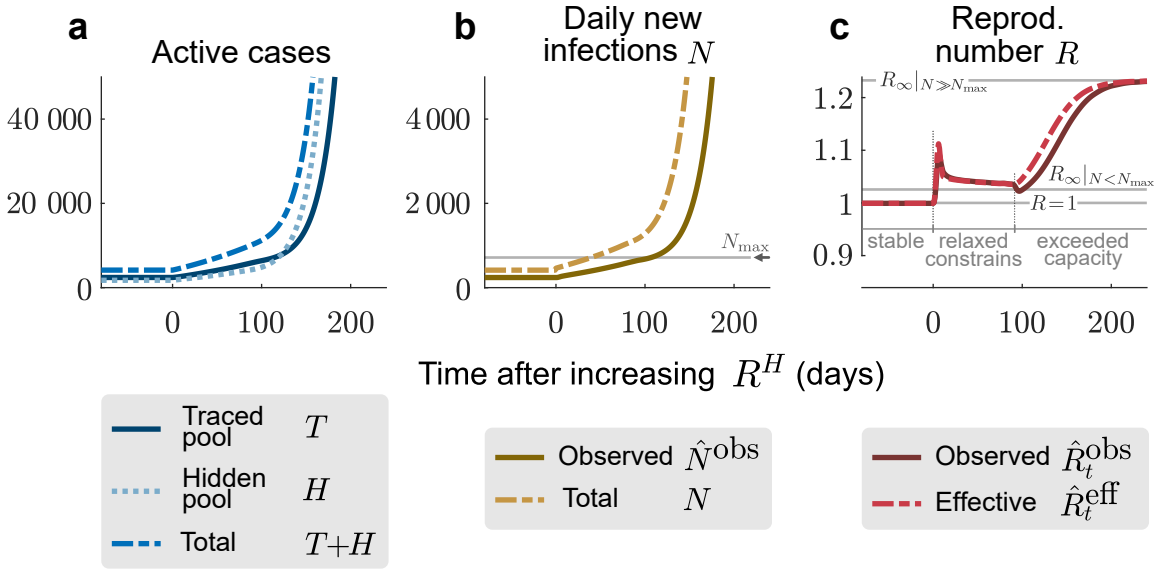


Figure 6: **A relaxation of restrictions can slowly overwhelm the finite tracing capacity and trigger a new outbreak. (a)** At $t = 0$, the hidden reproduction number increases from $R_t^H = 1.8$ to $R_t^H = 2.0$ (i.e. slightly above its critical value). This leads to a slow increase in traced active cases (solid blue line). **(b)** When the number of observed new cases (solid brown line) exceeds the tracing capacity limit $N_{\max}$ (solid grey line), the tracing system breaks down and the outbreak starts to accelerate. **(c)** After an initial transient at the onset of the change in R_t^H, the observed reproduction number (solid red line) faithfully reflects both the slight increase of the hidden reproduction number due to relaxation of contact constraints, and the strong increase after the tracing capacity (solid grey line) is exceeded at $t \approx 100$. All the curves plotted are obtained from numerical integration of equations (1) - (5).

Even without a large influx event, the tipping-over into instability can occur when a relaxation of contact restrictions causes a slow growth in case numbers. This slow growth will accelerate dramatically once the tracing capacity limit is reached – constituting a transition from a slightly unstable to a strongly unstable regime (Supplementary Fig. 5d). To illustrate this, we simulated an increase of the hidden reproduction number R_t^H (of a system in stable equilibrium) at $t = 0$, from the subcritical default value of $R_t^H = 1.8$ to a supercritical value $R_t^H = 2$, which renders the system slightly unstable (Fig. 6). At $t = 0$, the case numbers start to grow slowly until the observed number of new cases exceeds the tracing capacity limit $N_{\max}$. From thereon, the tracing system breaks down and the growth self-accelerates. This is reflected in the steep rise of new cases after day 100 – thus with a considerable delay after the change of R_t^H, i.e. the population's behavior.

Both the initial change in the hidden reproduction number and the breakdown of the tracing system are reflected in the observed reproduction number $\hat{R}_t^{\text{obs}}$ (Fig. 6c). It transits from stability ($\hat{R}_t^{\text{obs}} = 1$) to instability ($\hat{R}_t^{\text{obs}} > 1$). However, the absolute values of $\hat{R}_t^{\text{obs}}$ are not very indicative about the public's behavior (R_t^H), because already small changes in R_t^H can induce large transient changes in $\hat{R}_t^{\text{obs}}$. In our example, $\hat{R}_t^{\text{obs}}$ shows a strong deflection after $t = 0$, although R_t^H changes only slightly; later, at $t \approx 100$ it starts to ramp to a new value, although R_t^H did not change. This ramping is due to the tracing capacity $N_{\max}$ being exceeded, which causes an acceleration of the spread. $\hat{R}_t^{\text{obs}}$ finally approaches a new steady-state value, as sketched in Supplementary Fig. 5d. To summarize, deducing the stability of the spread from $\hat{R}_t^{\text{obs}}$ is challenging because $\hat{R}_t^{\text{obs}}$ reacts very sensitively to many types of transients. R_t^H, in contrast, would be a reliable indicator of true spreading behavior, but is not accessible easily.

Imperfect TTI requires some social distancing to control SARS-CoV-2

Above, we illustrated that a combination of symptom-driven testing and contact tracing can control the outbreak for a default reproduction number of $R_t^H = 1.8$. We now ask how efficient the TTI scheme and implementation must be to control the disease for a range of reproduction numbers— i.e. what TTI parameters are necessary to avoid the tipping over to $\hat{R}_t^{\text{eff}} > 1$. To this end, we perform linear stability analysis to calculate the critical reproduction number at which the tipping-over occurs (see equation (1) in the Supplementary

Information). When assessing stability not only for a single scenario along the R_t^H-axis, but for multiple parameter combinations, the tipping points turn into critical lines (or surfaces). Here, we examine how these critical lines depend on different combinations of symptom-driven testing, random testing, and contact tracing.

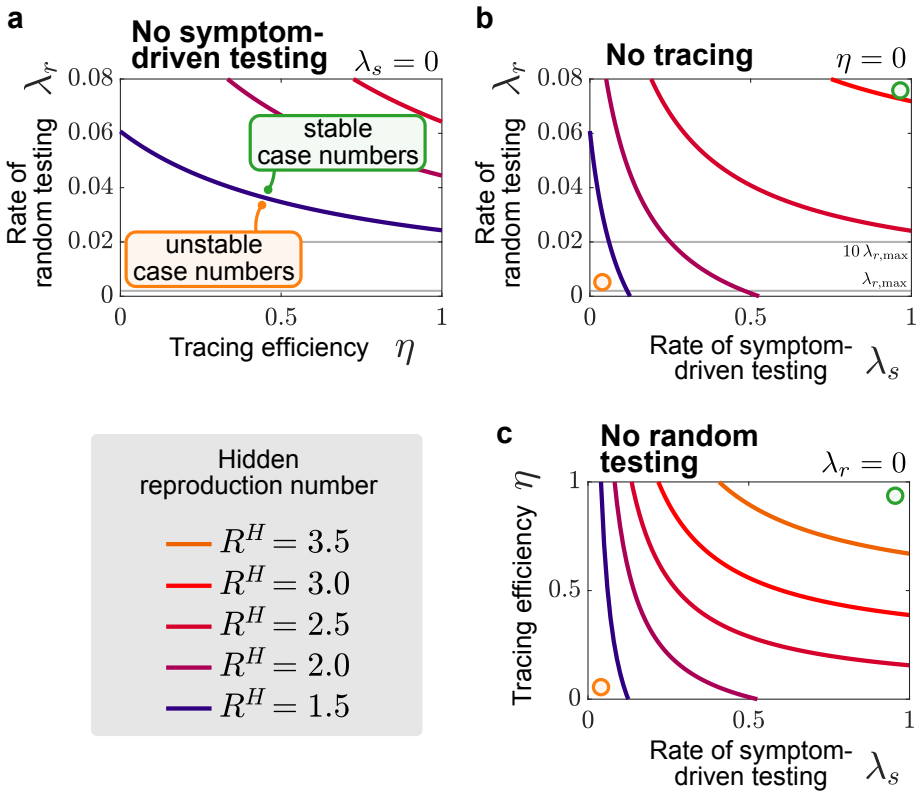


Figure 7: **Symptom-driven testing and contact tracing need to be combined to control the disease.** Stability diagrams showing the boundaries (continuous curves) between the stable (controlled) and uncontrolled regimes for different testing strategies combining random testing (rate λ_r), symptom-driven testing (rate λ_s), and tracing (efficiency η). Grey lines in plots with λ_r-axes indicate capacity limits (for our example Germany) on random testing ($\lambda_{r,\max}$) and when using pooling of ten samples, i.e. $10\lambda_{r,\max}$. Colored lines depict the transitions between the stable and the unstable regime for a given reproduction number R_t^H (colour-coded). The transition from *stable* to *unstable* case numbers is explicitly annotated for $R_t^H = 1.5$ in panel A. **(a)** Combining tracing and random testing without symptom-driven testing is in all cases not sufficient to control outbreaks, as the necessary random tests exceed even the pooled testing capacity ($10\lambda_{r,\max}$). **(b)** Combining random and symptom-driven testing strategies without any contract tracing requires unrealistically high levels of random testing to control outbreaks with large reproduction numbers in the hidden pool ($R_t^H > 2.0$). The required random tests to significantly change the stability boundaries exceed the available capacity in Germany $\lambda_{r,\max}$. Even taking into account the possibility of pooling tests ($10\lambda_{r,\max}$) often does not suffice to control outbreaks. **(c)** Combining symptom-driven testing and tracing suffices to control outbreaks with realistic testing rates λ_s and tracing efficiencies η for moderate values of reproduction numbers in the hidden pool, R_t^H, but fails to control the outbreak for large R_t^H. The curves showing the critical reproduction number are obtained from the linear stability analysis (equation (1)).

Random testing with tracing, but without symptom-driven testing ($\lambda_s = 0$), is not sufficient to contain an outbreak (under our default parameters and $R_t^H \leq 1.5$; Fig. 7a). This is because the rate of random testing λ_r would have to be unrealistically large. It exceeds the current capacity of testing ($\lambda_{r,\max} \sim 0.002$, see Methods for details), even if ten tests are pooled ($\lambda_r \sim 10\lambda_{r,\max}$ [25]). Thus, the contribution of symptom-driven testing is necessary to control any realistic new outbreak through TTI.

Contact tracing markedly contributes to outbreak mitigation (Fig. 7b). In its absence, i.e. when isolating only individuals that were positive in a symptom-driven or random test, the outbreak can be controlled for intermediate reproduction numbers ($R_t^H < 2.5$ in Fig. 7b) but not for higher ones if the limit of $\lambda_{r,\max} < 0.02$ is respected.

The most effective combination appears to be symptom-driven testing together with contact tracing (Fig. 7c). This combination shows stability even for spreads close to the basic reproduction number $R_t^H = R_0 \approx 3.3$ [1–3], when implemented extremely efficiently (e.g. with $\lambda_s = 0.66$ and $\eta = 0.66$). However, this implementation would require that all symptomatic persons get tested within 1-2 days after getting infectious, thus potentially already in their pre-symptomatic phase, which may be difficult to realize. (Note that the asymptomatic cases are already accounted for in the model and do not pose an additional problem). Considering these difficulties, the combination of symptom-driven testing and contact tracing appears to be sufficient to contain outbreaks with *intermediate* reproduction numbers ($R_t^H \sim 2$ can be controlled with e.g. $\lambda_s \leq 0.5$ and $\eta = 0.66$, Fig. 7c).

Overall, our model suggests that the combination of timely symptom-driven testing within very few days, together with isolation of positive cases and efficient contact tracing can be sufficient to control the spread of SARS-CoV-2 given the reproduction number in the hidden pool is $R_t^H \approx 2$ or lower. For random testing at the population level to be effective, one would require much higher test rates than currently available in Germany. Random testing nevertheless can be useful to control highly localized outbreaks, and is paramount for screening frontline workers in healthcare, eldercare and education.

How can TTI compensate the relaxation of contact constraints?

There are currently strong incentives to loosen restrictive measures and return more to a pre-COVID-19 lifestyle [28, 29]. Any such loosening, however, can lead to a higher reproduction number R_t^H, which could potentially exceed the critical value R_{crit}^H, for which current TTI strategies ensure stability. To retain stability despite increasing R_t^H, this increase has to be compensated by stronger mitigation efforts, such as further improvement of TTI. Thereby the critical value R_{crit}^H is effectively increased. In the following, we compare the capacity of the different TTI and model parameter changes to compensate for increases of the reproduction number R_t^H. In detail, we start from the highest reproduction number that can be controlled by the default parameters, $R_{\text{crit}}^H = 1.89$, and calculate how each model parameter would have to be changed to achieve a desired increase in R_{crit}^H. For all default parameters, see Table 1.

First, we explore how well an increase of random and symptom-driven test rates can compensate an increase in R_t^H (Fig. 8a). We find that population-wide random testing would need to increase extensively to compensate an increases in R_t^H, i.e. λ_r quickly exceeds realistic values (grey lines in Fig. 8a). Thus, random testing at the level of the whole population is not the most efficient tool to compensate increases of the hidden reproduction rate, but that does not diminish its usefulness in controlling localized outbreaks, or in the protection of frontline workers and highly vulnerable populations.

In contrast, scaling up symptom-driven testing can in principle compensate an increase of R_t^H up to about 3 (Fig. 8a). Beyond $R_t^H = 3$ and $\lambda_s \approx 0.4$, λ_s increases more steeply, making this compensation increasingly costly (Fig. 8a). Furthermore, levels of $\lambda_s > 0.5$ seem hard to realize as they would require testing within < 2 days of becoming infectious, i.e. while many infected are still pre-symptomatic. Realistically, only moderate increases in R_t^H can be compensated by decreasing the average delay of symptom-driven testing alone.

Tracing the contacts of an infected person and asking them to quarantine preventively is an important contribution to contain the spread of SARS-CoV-2, if done without delay [3, 13]. As a default, we assumed that a fraction $\eta = 0.66$ of contacts are traced and isolated within a day. This fraction can in principle be increased further to compensate an increase in R_t^H and still guarantee stability (Fig. 8a). However, because η is already high in the first place, its range is quite limited, and even perfect contact tracing cannot compensate an R_t^H of 2.5. More elaborate contact tracing strategies, like backward-forward tracing might further improve its effective efficacy.

As an alternative to improved TTI rates and efficiencies, improved compliance may compensate an increase in R_t^H: One might aim to reduce the number of contacts missed in the traced pool ϵ, improve the isolation factor ν, or reduce the fraction of people avoiding tests despite showing symptoms φ (Fig. 8c). These improvements might be more difficult to achieve from a policy-maker perspective but could be targeted by educational and awareness-raising campaigns. However, since we assumed already in the default scenario that the behavioral factors (ϵ, ν, φ) are not too large, the potential improvement is limited.

The amount of reduction achievable by each method is limited, which calls to leverage all these strategies together. Furthermore, as can be seen from the curvature of the lines in Fig. 7, the beneficial effects are synergistic, i.e. they are larger when combining several strategies instead of spending twice the efforts on a unique one. This synergy of improved TTI measures and awareness campaigning could allow to relax contact constraints while keeping outbreaks under control. Nonetheless, our model still indicates that compensating

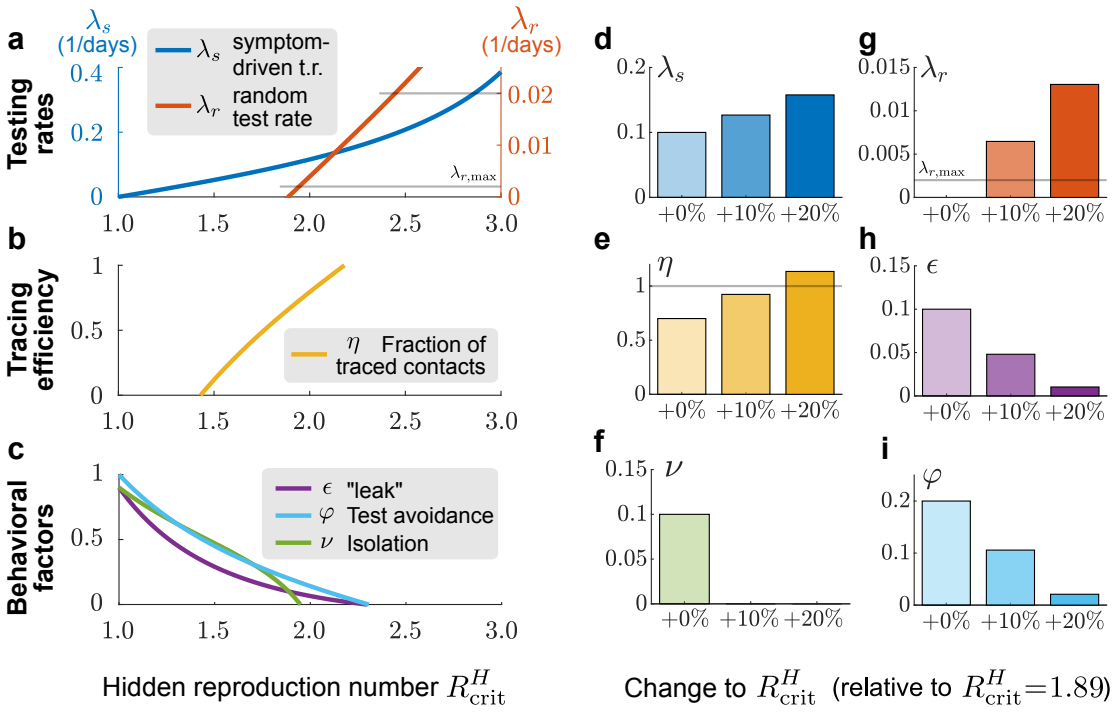


Figure 8: **Adapting testing strategies allows for relaxation of contact constraints to some degree.** The relaxation of contact constraints increases the reproduction number of the hidden pool R_t^H, and thus needs to be compensated by adjusting model parameters to keep the system stable. **(a-c)** Value of a single parameter required to keep the system stable despite a change in the hidden reproduction number, while keeping all other parameters at default values. **(a)** Increasing the rate of symptom-driven testing λ_s (blue) can in principle compensate for hidden reproduction numbers close to R_0. This is optimistic, however, as it requires that anyone with symptoms compatible with COVID-19 gets tested and isolated on average within 2.5 days – requiring large resources and efficient organization. Increasing the random-testing rate λ_r (red) to the capacity limit (for the example Germany, grey line $\lambda_{r,\max}$) would have almost no effect, pooling tests to achieve $10\lambda_{r,\max}$ can compensate partly for larger increases in R_t^H. **(b)** Increasing the tracing efficiency can compensate only small increases in R_t^H. **(c)** Decreasing the fraction of symptomatic individuals who avoid testing φ, the leak from the traced pool ϵ or the escape rate from isolation ν can in principle compensate for small increases in R_t^H. **(d-i)** To compensate a 10% or 20% increase of R_t^H, while still keeping the system stable, symptom-driven testing λ_s could be increased (d), or ϵ or φ could be decreased (h,i). In contrast, only changing λ_r, η, or ν would not be sufficient to compensate a 10 % or 20 % increase in R_t^H, because the respective limits are reached (e,f,g). All parameter changes are computed through stability analysis (equation (1)).

the basic reproduction number $R_t^H = R_0 \approx 3.3$ [1–3] might be very costly, and hence some degree of physical distancing might be required.

Robustness against parameter changes and model limitations

Above, we showed that changing the implementation of the TTI strategy can accommodate higher reproduction numbers R^H_{crit} – but how robust are these implementations against parameter uncertainties? To explore the robustness of the resulting hidden reproduction number R^H_{crit} against simultaneous variation of multiple TTI parameters, we draw these parameters from beta distributions (because all parameters are bounded by 0 and 1) centered on the default values and perform an error propagation analysis (Supplementary Table 1). We found that a hidden reproduction number of $R_t^H \leq 1.4$ (95 % CI, 1.23–1.69) can be compensated by testing alone, whereas additional contact tracing allows a hidden reproduction number of $R_t^H \leq 1.9$ (95 % CI, 1.42–2.70, Supplementary Fig. 2, Supplementary Table 1). This shows that the exact implementation of the TTI strategy strongly impacts the public behavior that can be controlled, but none of them allows for a complete lifting of contact restrictions ($R_0 = 3.3$).

Another aspect of robustness is not that against variation of parameters, but against variation of the model and the underlying assumptions. Our model also comes with some inevitable simplifications, but these

do not compromise the conclusions drawn here. Specifically, our model is simple enough to allow for a mechanistic understanding of its dynamics and analytical treatment of the control and stability problems. This remains true even when extending the model to incorporate more biological realism, e.g. the different transmissibility of asymptomatic and symptomatic cases (Supplementary Fig. 6). Owing to its simplicity it has certain limitations: In contrast to agent-based simulations [30, 31], we do not include realistic contact structures [4, 5, 32] - the infection probability is uniform across the whole population. This limitation will become relevant mostly when trying to devise even more efficient testing and tracing strategies, and when a stabilization of a system very close to its tipping point is desired. Compared to other mean-field based studies which included a more realistic temporal evolution of infectiousness [33, 34], we implicitly assume that infectiousness decays exponentially. This assumption has the disadvantage of making the interpretation of rate parameters more difficult, but should not have an effect on the stability analyses presented here.

Discussion

Using a compartmental SIR-type model with realistic parameters based on our example case Germany, we find that test-trace-and-isolate can, in principle, contain the spread of SARS-CoV-2 if some physical distancing measures are continued. We analytically derived the existence of a novel meta-stable regime of spreading dynamics governed by the limited capacity of contact tracing and show how transient perturbations can tip a seemingly stable system into the unstable regime. Furthermore, we explored the boundaries of this regime for different TTI strategies and efficiencies of the TTI implementation.

Our results are in agreement with other simulation and modeling studies investigating how efficient TTI strategies are in curbing the spread of the SARS-CoV-2. Both agent-based studies with realistic contact structures [4] and studies using mean-field spreading dynamics with tractable equations [33–37] agree that TTI measures are an important contribution to control the pandemic. Fast isolation is arguably the most crucial factor, which is included in our model in the testing rate λ_s. Yet, TTI is generally not perfect and the app-based solutions that have been proposed at present still lack the necessary large adoption that was initially foreseen, and that is necessary for these solutions to work [34]. Our work, as well as others [4, 34, 38, 39], show that realistic TTI can compensate reproduction numbers of around 1.5-2.5, which is however lower than the basic reproduction number of around 3.3 [1–3]. This calls for continued contact reduction on the order of 25–55 %, and it does not only highlight the importance of TTI, but also the need of other mitigation measures.

Our work extends previous studies by combining the explicit modeling of a hidden pool (including test avoiders) with the exploration of various ways of allocating testing and tracing resources. This allows us to investigate the effectiveness of various approaches to stabilize disease dynamics in the face of a relaxation of physical distancing. This yields important insights for policy makers into how to allocate resources. We also include a capacity limit of tracing, which is typically not included in other studies, but important to understand the meta-stable regime of a TTI-stabilized system, and to understand the importance of keeping a safety distance to the critical reproduction number of a given TTI strategy. Last, we highlight the important differences between the observed reproduction numbers — as they are reported in the media — and the more important, but hard to access, reproduction number in the hidden pool. Specifically we show how transient behavior of the observed reproduction number may be easily misinterpreted.

Limited TTI capacity implies a meta-stable regime with the risk of sudden explosive growth. Both, testing as well as tracing contribute to containing the spread of SARS-CoV-2. However, if their capacity limit is exceeded by the number of new infections, then an otherwise controlled spread becomes uncontrolled. This is particularly troubling because the spread is self-accelerating: the more the capacity limit is exceeded, the less testing and tracing can contribute to containment. To avoid this situation, the reproduction number has to stay below its critical value, and the number of new infections below TTI capacity. Therefore, it is advisable to maintain a safety margin to these limits. Otherwise, a small increase of the reproduction number, super-spreading events [40], or sudden influx of externally acquired infections e.g. after holidays, lead to uncontrolled spread. Re-establishing stability is then quite difficult.

As the number of available tests is limited, the relative efficiencies of random, symptom-driven and tracing-based testing should determine the allocation of resources [10]. The efficiency of test strategies in terms of positive rate is a primary metric to determine the allocation of tests [41]. Contact-tracing based testing will generally be the most efficient use of tests (positive rate on the order of $R_t^H/\{\text{number of contacts}\}$), especially in the regime of low contact numbers [37, 42]. The efficiency of symptoms-driven testing depends on the set of symptoms used for admission: Highly specific symptom sets will allow for a high yield, but

miss a number of cases (for instance, 33% of cases do not show a loss of smell/taste [43]). Unspecific symptom sets in contrast will require a high number of tests, especially in seasons where other respiratory conditions are prominent (currently, the fraction of SARS-CoV-2 cases among all influenza-like cases is less than 4% [44]). Random testing on a population level has the smallest positive rate in the regime of low prevalence that we focus on [41, 45], but could be used in a targeted manner, e.g. screening of healthcare workers, highly vulnerable populations [10, 46] or those living in the vicinity of localized outbreaks. We conclude that contact-tracing based testing and highly specific symptoms-based testing should receive the highest priority, with the remaining test capacity used on less specific symptoms-based testing and random screening in particular settings.

The cooperation of the general population in maintaining a low reproduction number is essential even with efficient TTI strategies in place. Our results illustrate that the reproduction number in the hidden pool R_t^H — which reflects the public's behavior — is still central to disease control. Specifically, we found that $R_t^H \leq 1.4$ (95 % CI, 1.23–1.69) can very likely be compensated by testing and isolating alone, whereas additional contract tracing shifts this boundary to $R_t^H \leq 1.9$ (95 % CI, 1.42–2.70, Supplementary Fig. 2, Supplementary Table 1). Both of these values are substantially lower than the basic reproduction number of SARS-CoV-2, $R_0 \approx 3.3$ [1–3]. Thus, if the goal is to contain the spread of SARS-CoV-2 with the available TTI-related resources, the reproduction number in the hidden pool will have to be reduced effectively by roughly $25 - 55\%$ compared to the beginning of the pandemic. This effective reduction may be achieved by a suitable combination of hygiene measures, such as mask wearing, filtering or exchange of contaminated air, and physical distancing. Useful accompanying measures on a voluntary basis include: immediately and strictly self-isolating upon any symptoms compatible with COVID-19, avoiding travel to any region with a higher infection rate, keeping a personal contact diary, using the digital tracing app, selecting only those contacts that are essential for one's well being, and avoiding contacts inside closed rooms if possible. Most of these measures and also an efficient tracing cannot be achieved without widespread cooperation of the population. This cooperation might be increased by a ramping up of coordinated educational efforts around explaining mechanisms and dynamics of disease spreading to a broad audience — instead of just providing behavioral advice.

The parameters of the model have been chosen to suit the situation in Germany. We expect our general conclusions to hold for other countries as well, but of course parameters would have to be adapted to local circumstances. For instance some Asia-Pacific countries can keep the spread under control employing mainly test-trace-and-isolate measures [47]. Factors which contribute to this are (1) significantly larger investment in tracing capacity, (2) a smaller influx of externally acquired infections (especially in the case of new Zealand) and (3) the wider acceptance of mask-wearing and compliance with physical distancing measures. These countries illustrate that even once "control is lost" in the sense of our model, it can in principle be regained trough political measures. A currently discussed mechanism to regain control is the "circuit breaker", a relatively strict lockdown to interrupt infection chains and bring case number down [48]. Such a circuit breaker or reset is particularly effective if it brings the system below the tipping point and thereby enables controlling the spread by TTI again.

To conclude, based on a simulation of disease dynamics influenced by realistic TTI strategies with parameters taken from the example of Germany, we show that the spreading dynamics of SARS-CoV-2 can only be stabilized if effective TTI-strategies are combined with hygiene and physical distancing measures that keep the reproduction number in the general population below a value of approximately $R_t^H \leq 1.9$ (95 % CI, 1.42–2.70). As a system stabilized by TTI with a finite capacity is only in a meta-stable state and can be tipped into instability by one-time effects, it would be desirable to keep a safety distance even to these values, if possible. The above bounds on the reproduction number in the hidden pool can be easily recomputed for other countries with different TTI capacities and reproduction numbers.

Methods

Model overview. We model the spreading dynamics of SARS-CoV-2 as the sum of contributions from two pools, i.e. traced T and hidden H infections (see sketch in Fig. 1). The first pool (T) contains traced cases revealed through testing or by contact tracing of an individual that has already been tested positive; all individuals in the traced pool are assumed to isolate themselves (quarantine), avoiding further contacts as well as possible. In contrast, in the second pool, infections spread silently, and only become detected when individuals develop symptoms and get tested, or via random testing in the population. This second pool (H) is therefore called the hidden pool H; individuals in this pool are assumed to exhibit the behavior of the general population, thus of everyone who is not aware of being infected. We model the mean-field interactions

between the hidden and the traced pool by transition rates which determine the timescales of dynamics of the mode. These transition rates can implicitly incorporate both the time course of the disease and the delays inherent to the TTI process, but we do not explicitly model delays between compartments. We distinguish between symptomatic and asymptomatic carriers – this is central when exploring different testing strategies (as detailed below). We also include effects of non-compliance and imperfect contact tracing, as well as a non-zero influx Φ of new cases which acquired the virus from outside. As this influx makes an eradication of SARS-CoV-2 impossible, only an exponential growth of cases or a stable rate of new infections are possible modeling outcomes. Given the two possible behaviours of the system, indefinite growth or stable cases, we frame our investigation as a stability problem, where the aim is to implement test-trace-and-isolate strategies in a way that allows the system to remain stable.

Spreading Dynamics

Concretely, we use a modified SIR-type model, where infections I are either symptomatic (I^s) or asymptomatic (I^a), and they belong to the hidden (H) or a traced (T) pool of infections (Fig. 1), thus creating in total four compartments of infections (H^s, H^a, T^s, T^a). New infections are asymptomatic with a ratio ξ^{ap}, the others are symptomatic. In all compartments individuals are removed with a rate Γ because of recovery or death (see Tab. 1 for all parameters).

In the hidden pool, the disease spreads according to the reproduction number R_t^H. This reproduction number reflects the disease spread in the general population, without testing induced isolation of individuals. In addition, the hidden pool receives a mobility-induced influx Φ of new infections. Cases are removed from the hidden pool (i) when detected by TTI, and put into the traced pool, or (ii) due to recovery or death.

The traced pool T contains those infected individuals who have been tested positive as well as their positively tested contacts. As these individuals are (imperfectly) isolated, they cause infections with a rate $\nu\Gamma R_t^H$, which are subsequently isolated and therefore stay in the traced pools and additional infections with a rate $\epsilon\Gamma R_t^H$, which are missed and act as an influx to the hidden pools. ν is the isolation factor and ϵ is the leak factor. The overall reproduction number of the traced pool is therefore $R_t^T = (\nu + \epsilon)\, R_t^H$.

In the scope of our model, it is important to differentiate exchanges from pool to pool that are based either on the "reassignment" of individuals or on infections. To the former category belongs the testing and tracing, which transfer cases from the hidden pool to the traced pool. These transfers involve a subtraction and addition of case numbers in the respective pools. To the latter category belongs the recurrent infections ΓR_t^H or $\nu\Gamma R_t^H$ and the 'leak' infections $\epsilon\Gamma R_t^H$. Exchanges of this category involves only an addition of case numbers in the respective pool.

Within our model, we concentrate on the case of low incidence and low fraction of immune people, as in the early phase of any new outbreak. Our model can also reflect innate or acquired immunity; one then has to rescale the population or the reproduction number. The qualitative behavior of the dynamics is not expected to change.

Parameter Choices and Scenarios

For any testing strategy, the fraction of infections that do not develop any symptoms across the whole infection timeline is an important parameter, and this also holds for testing strategies applied to the case of SARS-CoV-2. In our model this parameter is called ξ^{ap} and includes beside true asymptomatic infections ξ also the fraction of individuals that avoid testing φ.

The exact value of the fraction of asymptomatic infections ξ, however, is still fraught with uncertainty, and it also depends on age [15, 49, 50]. While early estimates were as high as 50 % (for example ranging from 26 % to 63 % [51]), these early estimates suffered from reporting bias, small sample sizes and sometimes included pre-symptomatic cases as well [22, 52]. Recent bias-corrected estimates from large sample sizes range between 12 % [22] and 33 % [23]. We decided to use 15 % for the pure asymptomatic ratio ξ.

In addition, we include a fraction φ of individuals avoiding testing. This can occur because individuals do not want to be in contact with governmental authorities or because they deem risking a spread of SARS-CoV-2 less important than having to quarantine [16]. As this part of the population may act in the same manner as asymptomatic persons, we include it in the asymptomatic compartment of the hidden pool, assuming a value of 0.2. We thus arrive at an effective ratio of asymptomatic infections $\xi^{\mathrm{ap}} = \xi + (1 - \xi)\varphi = 0.32$. We assume that both, symptomatic and asymptomatic persons, have the same reproduction number.

In general, infected individuals move from the hidden to the traced pool after being tested; yet, also a small number of infections will leak from the traced to the hidden pool with rate $\epsilon\Gamma R_t^H$, with $\epsilon = 0.1$. A source of leak would be a contact that has been infected, traced and tested positive, but still ignores quarantine instructions. For the model, this individual has the same effect on disease dynamics as someone from the hidden pool.

Another crucial parameter for any TTI strategy is the reproduction number in the hidden pool R_t^H. This parameter is by definition impossible to measure, but it presents typically the main driver of the spreading dynamics. It depends mainly on the contact behavior of the population, and ranges from R_0 in the absence of contact restrictions to values below 1 during strict lock-down [2]. For the default parameters of our model, we used a value of $R_t^H = 1.8$. This parameter was chosen after all others, aiming to mirror the epidemic situation in Germany during the early summer months, when infections remained approximately constant. It is just below the critical value $R_{\text{crit}}^H = 1.98$ for the default scenario, hence $\hat{R}_t^{\text{eff}} = 1$. This value of $R_t^H = 1.8$ is about 54 % lower than the basic reproduction number $R_0 \approx 3.3$, hence we assume that some non-pharmacological interventions (physical distancing or hygiene measures) are in place, as was the case in Germany during the early summer months [1, 2]. For additional scenarios, we explored the impact of both higher and lower values of R_t^H on our TTI strategy (see Figures 7, 8 and Supplementary Figure 2).

Testing-and-Tracing strategies

We consider three different testing-and-tracing strategies: random testing, symptom-driven testing and specific testing of traced contacts. Despite the naming — chosen to be consistent with existing literature [4,36,42,53,54]— an isolation of the cases tested positive is part of all of these strategies. The main differences lie in whom the tests are applied to and whether past contacts of an infected person are traced and told to isolate. Our model simulates the parallel application of all three strategies – as it is typical for real-world settings, and yields the effects of the "pure" application of these strategies as corner cases realized via specific parameter settings.

Random testing is defined here as applying tests to individuals irrespective of their symptom status, or whether they belonging to the contact-chain of other infected individuals. In our model, random testing transfers infected individuals from the hidden to the traced pool with fixed rate λ_r, irrespective of them showing symptoms or not. In reality, random testing is often implemented as situation-based testing for a sub-group of the population, e.g. at a hot-spot, for groups at risk, or for people returning from travel. Such situation-based strategies would be more efficient than the random testing assumed in this model. Nonetheless, because random testing can detect symptomatic and asymptomatic persons alike, we decided to evaluate its potential contribution to contain the spread.

The number of random tests that can be performed is limited by the available laboratory and sample collection capacity. For orientation, we included therefore a maximal testing capacity of $\lambda_{r,\max} = 0.002$ test per person and day, which reflects the laboratory capacity in Germany (1.2 Mio. per week) [55, 56]. Potentially, the testing capacity can be increased by pooling PCR-tests, without strongly reducing the sensitivity [25]. We acknowledge this possibility by also taking into account a ten times larges testing capacity, $10 \cdot \lambda_{r,\max} = 0.02$. This would correspond to every person being tested on average every 50 days (7 weeks) - summing to about 12 Mio. tests per week in Germany.

Symptom-driven testing is defined as applying tests to individuals presenting symptoms of COVID-19. In this context, it is important to note that non-infected individuals can have symptoms similar to those of COVID-19, as many symptoms are rather unspecific. Although symptom-driven testing suffers less from imperfect specificity, it can only uncover symptomatic cases that are willing to be tested (see below). Here, *symptomatic infected individuals* are transferred from the hidden to the traced pool at rate λ_s.

We define λ_s as the daily rate at which symptomatic individuals get tested, among the subset who are willing to get tested. As default value we use $\lambda_s = 0.1$, which means that one in ten people that show symptoms gets tested each day and are subsequently isolated. Testing and isolation happens immediately in this model, but their report into the observed new daily cases $\hat{N}^{\text{obs}}$ is delayed. Further real-world delays can effectively be modelled by a lower effective λ_s. In theory, this rate could be increased to one per day. However, this parameter range is on purpose not simulated here. For SARS-CoV-2, such a fast detection is unrealistic, because typically infected people show a the delay of 1-2 days between the beginning of infectiousness and showing symptoms [57]. Hence, $\lambda_s \approx 0.5$ is an upper limit to the symptom-driven testing rate.

Tracing contacts of positively tested individuals presents a very specific test strategy, and is expected to be effective in breaking the infection chains, if contacts self-isolate sufficiently quickly [4, 42, 58]. However as

every implementation of a TTI strategy is bound to be imperfect, we assume that only a fraction $\eta < 1$ of all contacts can be traced. These contacts, if tested positive, are then transferred from the hidden to the traced pool. No delay is assumed here. The parameter η effectively represents the fraction of secondary and tertiary infections that are found through contact-tracing. As this fraction decreases when the delay between testing and contact-tracing increases we assumed a default value of $\eta = 0.66$, i.e. on average only two thirds of subsequent infections are prevented.

Contact tracing is mainly done by the health authorities in Germany, and this clearly limits the maximum number $N_{\max}$ of observed new cases $\hat{N}^{\text{obs}}$, for which contact tracing is still functional. In the first part of the manuscript, we assume for simplicity that $\hat{N}^{\text{obs}}$ is sufficiently small to not exceed the tracing capacity; in the second part, we explicitly explore the role of this limit.

In principle, the tracing capacity limit can be expressed in two ways, either as the number of observed cases $\hat{N}^{\text{obs}}$, at which tracing starts to break down (denoted by $N_{\max}$), or as number of positive contacts that can maximally be detected and handled on average by the health departments ($n_{\max}$). Both values depend strongly on the personnel capacity of the health departments and the population's contact behavior. From the system's equilibrium equations, we derive a linear relation between the two, with the proportionality being a function of the epidemiological and TTI parameters (Supplementary Equation 14). For simplicity, we only use $N_{\max}$ in the main text and refer the interested reader to the derivation in Supplementary Information Section 2.

As a default value, we assume $n_{\max} = 300$ positive contacts that can be handled per day. This corresponds to $N_{\max} = 718$ observed cases per day, from which the above-mentioned 300 cases where found through contact tracing and the remaining 418 either originate within the traced pool (e.g. infected family members), or where found through symptom-based testing and are therefore considered to be detected with much less effort. This limit of $n_{\max} = 300$ is currently well within reach of the 400 health departments in Germany. At first sight, this limit may appear low (about one case per working day per health department). However, identifying, contacting and counselling all contact persons (thus many more persons than 300), and finally testing them and controlling their quarantine requires considerable effort.

Any testing can in principle produce both false-positive (quarantined individuals who were not infected) and false-negative (non-quarantined infected individuals) cases. False-positive rates in theory should be very low (0.2 % or less for RT-PCR tests). However, testing and handling of the probes can induce false-positive results [59, 60]. Under low prevalence of SARS-CoV-2, false-positive could therefore outweigh true-positive, especially for the random testing strategy, where the number of tests required to detect new infections would be very high [61, 62]. This should be carefully considered when choosing an appropriate testing strategy, but has not been explicitly modeled here, as it does not contribute strongly to whether or not the outbreak could be controlled.

Model Equations

The contributions of the spreading dynamics and the TTI strategies are summarized in the equations below. They govern the spreading dynamics of case numbers in and between the hidden and the traced pool, H and T. We assume a regime of low prevalence and low immunity, i.e. the majority of the population is susceptible. Thus, the dynamics are completely determined by spread (characterized by the reproduction numbers R_t), recovery (characterized by the recovery rate Γ), external influx Φ and the impact of the TTI strategies:

$$\frac{dT}{dt} = \underbrace{\Gamma\left(\nu R_t^H - 1\right) T}_{\text{spreading dynamics}} + \underbrace{\lambda_s H^s + \lambda_r H}_{\text{testing}} + \underbrace{f\left(H^s, H\right)}_{\text{tracing}} , \tag{1}$$

$$\frac{dH}{dt} = \underbrace{\Gamma\left(R_t^H - 1\right) H}_{\text{spreading dynamics}} - \underbrace{\left(\lambda_s H^s + \lambda_r H\right)}_{\text{testing}} - \underbrace{f\left(H^s, H\right)}_{\text{tracing}} + \underbrace{\Gamma\epsilon R_t^H T}_{\text{missed contacts}} + \underbrace{\Phi}_{\text{external influx}} , \tag{2}$$

$$\frac{1}{1-\xi^{\text{ap}}}\frac{dH^s}{dt} = \underbrace{\Gamma\left(R_t^H H - \frac{H^s}{1-\xi^{\text{ap}}}\right)}_{\text{spreading dynamics}} - \underbrace{\frac{\left(\lambda_s + \lambda_r\right) H^s}{1-\xi^{\text{ap}}}}_{\text{testing}} - \underbrace{f\left(H^s, H\right)}_{\text{tracing}} + \underbrace{\Gamma\epsilon R_t^H T}_{\text{missed contacts}} + \underbrace{\Phi}_{\text{external influx}} , \tag{3}$$

$$H^a = H - H^s, \tag{4}$$

$$\text{with } f(H^s, H) = \min\left\{n_{\max}, \eta R_t^H \left(\lambda_s H^s + \lambda_r H\right)\right\}. \tag{5}$$

Equations (1) and (2) describe the dynamical evolution of both the traced and hidden pools. They are however not sufficient to completely describe the underlying dynamics of the system in the hidden pool, as the symptomatic and asymptomatic subpools behaves slightly different: only from the symptomatic hidden pool (H^s) cases can be removed because of symptom-driven testing. Thus the specific dynamics of H^s is defined by equation (3). The dynamics of the asymptomatic hidden pool (H^a) can be inferred from equation (4). In the traced compartment, the asymptomatic and symptomatic pools do not need to be distinguished, as their behavior is assumed to be identical. Equation (5) reflects a potential limit $n_{\max}$ of the tracing capacity of the health authorities. It is expressed as the total number of positive cases that can be detected from tracing the contacts of people who were detected via symptom-driven testing (from H^s) or via random testing (from H).

Central epidemiological parameters that can be observed

In the real world, the disease spread can only be observed by the traced pool. While the *true* number of daily infections N is a sum of all new infections in the hidden and traced pools, the *observed* number of daily infections $\hat{N}^{\text{obs}}$ is the number of new infections in the traced pool delayed by a variable reporting delay α. This includes internal contributions and contributions from testing and tracing:

$$N(t) = \underbrace{\Gamma\left(\nu + \epsilon\right) R_t^H T(t)}_{\text{traced pool}} + \underbrace{\Gamma R_t^H H(t)}_{\text{hidden pool}} + \underbrace{\Phi}_{\text{external influx}} \tag{6}$$

$$\hat{N}^{\text{obs}}(t) = \Big[\underbrace{\Gamma\nu R_t^H T(t)}_{\text{traced pool}} + \underbrace{\lambda_s H^s(t) + \lambda_r H(t)}_{\text{testing}} + \underbrace{f(H^s(t), H(t))}_{\text{tracing}}\Big] \circledast \mathcal{G}[\alpha = 4, \beta = 1](t), \tag{7}$$

where $f(H^s, H)$ is defined in (5), $\circledast$ denotes a convolution and $\mathcal{G}$ a Gamma distribution that models a variable reporting delay. The spreading dynamics are usually characterized by the observed reproduction number $\hat{R}_t^{\text{obs}}$, which is calculated from the observed number of new cases $\hat{N}^{\text{obs}}(t)$. We here use the definition underlying the estimates that are published by Robert-Koch-Institute, the official body responsible for epidemiological control in Germany [63]: the reproduction number is the relative change of daily new cases N separated by 4 days (the assumed serial interval of COVID-19 [64]):

$$\hat{R}_t^{\text{obs}} = \frac{\hat{N}^{\text{obs}}(t)}{\hat{N}^{\text{obs}}(t-4)} \tag{8}$$

$$\hat{R}_t^{\text{eff}} = \frac{N(t)}{N(t-4)} \tag{9}$$

While only $\hat{R}_t^{\text{obs}}$ is accessible from the observed new cases, in the model one can also define an effective reproduction number $\hat{R}_t^{\text{eff}}$ from the total number of daily new infections.

In contrast to the original definition of $\hat{R}_t^{\text{obs}}$ [63], we do not need to remove real-world noise effects by smoothing this ratio.

Numerical calculation of solutions and critical values.

The numerical solution of the differential equations governing our model were obtained using a versatile solver based on an explicit Runge-Kutta (4,5) formula, `@ode45`, implemented in MATLAB (version 2020a), with default settings. This algorithm allows the solution of non-stiff systems of differential equations in the shape $y' = f(t, y)$, given a user-defined time-step (for us, 0.1 days). Suitability and details on the algorithm are further discussed in [65].

To derive the tipping point between controlled and uncontrolled outbreaks (e.g. critical values of R_t^H), and to plot the stability diagrams, we used the `@fzero` MATLAB function. This function uses a combination of bisection, secant, and inverse quadratic interpolation methods to find the roots of a functions. For instance, following the discussion of Supplementary Section 1, R_{crit}^H was determined by finding the roots of the function returning the real part of the linear system's largest eigenvalue.

Table 1: Model parameters.

Parameter	Meaning	Value (default)	Range	Units	Source
M	Population size	80 000 000		people	Assumed
R_t^H	Reproduction number (hidden)	1.80		–	[2, 66, 67]
Γ	Recovery rate	0.10	0.08–0.12	day^{-1}	[57, 68, 69]
ξ	Asymptomatic ratio	0.15	0.12–0.33	–	[22, 23]
φ	Fraction skipping testing	0.20	0.10–0.40	–	[16]
ν	Isolation factor (traced)	0.10		–	Assumed
λ_r	random-testing rate	0	0–0.02	day^{-1}	Assumed
λ_s	symptom-driven testing rate	0.10	0–1	day^{-1}	Assumed
η	Tracing efficiency	0.66		–	Assumed
$N_{\max}$	Maximal tracing capacity	≈ 718	200–6000	$\text{cases}\,\text{day}^{-1}$	Assumed[1]
ϵ	Missed contacts (traced)	0.10		–	Assumed
Φ	Influx rate (hidden)	15		$\text{cases}\,\text{day}^{-1}$	Assumed[2]
$\lambda_{r,\max}$	Maximal test capacity per capita	0.002		cases day^{-1}	[55, 56]
R_t^T	Reproduction number (traced)	0.36		–	$R_t^T = (\nu + \epsilon)\, R_t^H$
ξ^{ap}	Apparent asymptomatic ratio	0.32		–	$\xi^{\text{ap}} = \xi + (1 - \xi)\varphi$
R^H_{crit}	Critical reproduction number (hidden)	1.89		–	Numerically calculated from model parameters

[1]Chosen for a country with a population of $M = 80 \cdot 10^6$. See methods for considerations.

Table 2: Model variables.

Variable	Meaning	Units	Explanation
H^a	Hidden asymptomatic pool	people	Non-traced, non-isolated people who are asymptomatic or avoid being tested
H^s	Hidden symptomatic pool	people	Non-traced, non-isolated people who are symptomatic
T^a	Traced asymptomatic pool	people	Known infected and isolated people who are asymptomatic
T^s	Traced symptomatic pool	people	Known infected and isolated people who are symptomatic
H	Hidden pool	people	Total non-traced people: $H = H^a + H^s$
T	Traced pool	people	Total traced people: $T = T^a + T^s$
N	New infections (traced and hidden)	$\text{cases}\,\text{day}^{-1}$	Given by: $N = \Gamma\,(\nu + \epsilon)\, R_t^H T + \Gamma R_t^H H + \Phi$
$\hat{N}^{\text{obs}}$	Observed new infections (influx to traced pool)	$\text{cases}\,\text{day}^{-1}$	Only cases of the traced pool; delayed on average by 4 days because of reporting
$\hat{R}_t^{\text{eff}}$	Estimated effective reproduction number	–	Estimated from the cases of all pools: $\hat{R}_t^{\text{eff}} = N(t)/N(t-4)$
$\hat{R}_t^{\text{obs}}$	Observed reproduction number	–	The reproduction number that can be estimated only from the observed cases: $\hat{R}_t^{\text{obs}} = \hat{N}^{\text{obs}}(t)/\hat{N}^{\text{obs}}(t-4)$

Data availability

Data used in this study was obtained through numerical simulation, and it is available together with the code for solving our model's equations for default and user-customized parameters at `https://github.com/Priesemann-Group/covid19_tti`. Alternatively, an interactive platform for simulating scenarios different from the herein presented is available on `http://covid19-tti.ds.mpg.de`, and users may download the data generated.

Code availability

We provide the code for generating graphics and all the different analyses included in both this manuscript and its Supplementary Information at `https://github.com/Priesemann-Group/covid19_tti`. An interactive platform for simulating scenarios different from the herein presented is available on `http://covid19-tti.ds.mpg.de`.

References

[1] Brauner, J. M. *et al.* The effectiveness and perceived burden of nonpharmaceutical interventions against COVID-19 transmission: a modelling study with 41 countries. Preprint at URL `https://doi.org/10.1101/2020.05.28.20116129` (2020)

[2] Dehning, J. *et al.* Inferring change points in the spread of COVID-19 reveals the effectiveness of interventions. *Science* **369**, 6500 (2020).

[3] Salathé, M. *et al.* COVID-19 epidemic in Switzerland: on the importance of testing, contact tracing and isolation. *Swiss medical weekly* **150**, w20225 (2020).

[4] Kucharski, A. J. *et al.* Effectiveness of isolation, testing, contact tracing, and physical distancing on reducing transmission of SARS-CoV-2 in different settings: a mathematical modelling study. *The Lancet Infectious Diseases* **0** (2020).

[5] Ruktanonchai, N. W. *et al.* Assessing the impact of coordinated COVID-19 exit strategies across Europe. *Science* **369**, 6510 (2020).

[6] Alwan, N. A. *et al.* Scientific consensus on the COVID-19 pandemic: we need to act now. *The Lancet* **6736**, 19–20 (2020).

[7] Lee, V. J., Chiew, C. J. & Khong, W. X. Interrupting transmission of COVID-19: lessons from containment efforts in Singapore. *Journal of Travel Medicine* **27**, taaa039 (2020).

[8] Pung, R. *et al.* Investigation of three clusters of COVID-19 in Singapore: implications for surveillance and response measures. *The Lancet* **395**, 1039-1046 (2020).

[9] Kang, J. *et al.* South Korea's Reponses to Stop the COVID-19 Pandemic. *American Journal of Infection Control* **48**, 1080-1086 (2020).

[10] Emanuel, E. J. *et al.* Fair allocation of scarce medical resources in the time of COVID-19 *New England Journal of Medicine* **382**, 2049-2055 (2020).

[11] Li, G., Li, W., He, X. & Cao, Y. Asymptomatic and presymptomatic infectors: hidden sources of COVID-19 disease. *Clinical Infectious Diseases* **418** (2020).

[12] Ye, F. *et al.* Delivery of infection from asymptomatic carriers of COVID-19 in a familial cluster. *International Journal of Infectious Diseases* **94**, 133-138 (2020).

[13] Kretzschmar, M., Rozhnova, G. & van Boven, M. Effectiveness of isolation and contact tracing for containment and slowing down a COVID-19 epidemic: a modelling study. *Available at SSRN 3551343* (2020).

[14] Rothe, C. *et al.* Transmission of 2019-nCoV infection from an asymptomatic contact in Germany. *New England Journal of Medicine* **382**, 970–971 (2020).

[15] Lai, C.-C. *et al.* Asymptomatic carrier state, acute respiratory disease, and pneumonia due to severe acute respiratory syndrome coronavirus 2 (SARS-CoV-2): facts and myths. *Journal of Microbiology, Immunology and Infection* **53**, 404-412 (2020).

[16] McDermott, J. H. & Newman, W. G. Refusal of viral testing during the SARS-CoV-2 pandemic. *Clinical Medicine* **20**, e163-e164 (2020).

[17] Linka, K., Rahman, P., Goriely, A. & Kuhl, E. Is it safe to lift COVID-19 travel bans? The Newfoundland story. *Computational Mechanics* **66**, 1081-1092 (2020).

[18] Panovska-Griffiths, J. *et al.* Determining the optimal strategy for reopening schools, work and society in the UK: balancing earlier opening and the impact of test and trace strategies with the risk of occurrence of a secondary COVID-19 pandemic wave. *The Lancet Child & Adolescent Health* **4**, 817-827 (2020).

[19] Kermack, W. O. & McKendrick, A. G. A contribution to the mathematical theory of epidemics. *Proceedings of the royal society of london. Series A, Containing papers of a mathematical and physical character* **115**, 700–721 (1927).

[20] Hethcote, H. W. An immunization model for a heterogeneous population. *Theoretical population biology* **14**, 338–349 (1978).

[21] Liu, Y., Gayle, A. A., Wilder-Smith, A. & Rocklöv, J. The reproductive number of COVID-19 is higher compared to SARS coronavirus. *Journal of travel medicine* **27**, taaa021 (2020).

[22] Byambasuren, O. *et al.* Estimating the extent of true asymptomatic COVID-19 and its potential for community transmission: systematic review and meta-analysis. *Official Journal of the Association of Medical Microbiology and Infectious Disease Canada* **30** (2020).

[23] Pollán, M. *et al.* Prevalence of SARS-CoV-2 in Spain (ENE-COVID): a nationwide, population-based seroepidemiological study. *The Lancet* **396**, 535-544 (2020).

[24] Rising, D. Coronavirus positive? Thousands in Germany left wondering *The Washington Post* (2020).

[25] Lohse, S. *et al.* Pooling of samples for testing for SARS-CoV-2 in asymptomatic people. *The Lancet Infectious Diseases* **20**, 1231-1232 (2020).

[26] Alimohamadi, Y. *et al.* Estimate of the Basic Reproduction Number for COVID-19: A Systematic Review and Meta-analysis. *J Prev Med Public Health* **53**, 151–157 (2020).

[27] Barber, A. *et al.* The basic reproduction number of SARS-CoV-2: a scoping review of available evidence. Preprint at URL `https://doi.org/10.1101/2020.07.28.20163535` (2020).

[28] Bonaccorsi, G. *et al.* Economic and social consequences of human mobility restrictions under COVID-19. *Proceedings of the National Academy of Sciences* **117**, 15530–15535 (2020).

[29] Rowthorn, R. & Maciejowski, J. A cost-benefit analysis of the COVID-19 disease. *Oxford Review of Economic Policy* **36**, S38–S55 (2020).

[30] Kerr, C. C. *et al.* Covasim: an agent-based model of COVID-19 dynamics and interventions. Preprint at URL `https://doi.org/10.1101/2020.05.10.20097469` (2020).

[31] Jalayer, M., Orsenigo, C. & Vercellis, C. CoV-ABM: A stochastic discrete-event agent-based framework to simulate spatiotemporal dynamics of COVID-19. Preprint at URL `https://arxiv.org/abs/2007.13231` (2020).

[32] Meloni, S. *et al.* Modeling human mobility responses to the large-scale spreading of infectious diseases. *Scientific reports* **1**, 62 (2011).

[33] Fraser, C., Riley, S., Anderson, R. M. & Ferguson, N. M. Factors that make an infectious disease outbreak controllable. *Proceedings of the National Academy of Sciences* **101**, 6146–6151 (2004).

[34] Ferretti, L. *et al.* Quantifying SARS-CoV-2 transmission suggests epidemic control with digital contact tracing. *Science* **368**, 6491 (2020).

[35] Lunz, D., Batt, G. & Ruess, J. To isolate, or not to isolate: a theoretical framework for disease control via contact tracing. Preprint at URL `https://doi.org/10.1101/2020.05.26.20113340` (2020).

[36] Sturniolo, S., Waites, W., Colbourn, T., Manheim, D. & Panovska-Griffiths, J. Testing, tracing and isolation in compartmental models. Preprint at URL `https://doi.org/10.1101/2020.05.14.20101808` (2020).

[37] Colbourn, T. *et al.* Modelling the Health and Economic Impacts of Population-Wide Testing, Contact Tracing and Isolation (PTTI) Strategies for COVID-19 in the UK. Preprint at URL `http://dx.doi.org/10.2139/ssrn.3627273` (2020).

[38] Hellewell, J. *et al.* Feasibility of controlling COVID-19 outbreaks by isolation of cases and contacts. *The Lancet Global Health* **8**, E488-E496 (2020).

[39] Davis, E. L. *et al.* An imperfect tool: COVID-19'test & trace' success relies on minimising the impact of false negatives and continuation of physical distancing. Preprint at URL `https://doi.org/10.1101/2020.06.09.20124008` (2020).

[40] Althouse, B. M. *et al.* Stochasticity and heterogeneity in the transmission dynamics of SARS-CoV-2. Preprint at URL `https://arxiv.org/abs/2005.13689` (2020).

[41] Kasy, M. & Teytelboym, A. Adaptive targeted infectious disease testing. *Oxford Review of Economic Policy* **36**, S77–S93 (2020).

[42] Firth, J. A. *et al.* Combining fine-scale social contact data with epidemic modelling reveals interactions between contact tracing, quarantine, testing and physical distancing for controlling COVID-19. Preprint at URL `https://doi.org/10.1101/2020.05.26.20113720` (2020).

[43] Chen, A. *et al.* Are Gastrointestinal Symptoms Specific for Coronavirus 2019 Infection? A Prospective Case-Control Study From the United States. *Gastroenterology* **159**, 1161–1163.e2. (2020).

[44] Arbeitsgemeinschaft Influenza Influenza-Monatsbericht. URL `https://influenza.rki.de/Wochenberichte/2019_2020/2020-32.pdf` (2020).

[45] Cleevely, M., Susskind, D., Vines, D., Vines, L. & Wills, S. A workable strategy for COVID-19 testing: stratified periodic testing rather than universal random testing. *Oxford Review of Economic Policy* **36**, S14–S37 (2020).

[46] Rivett, L. *et al.* Screening of healthcare workers for SARS-CoV-2 highlights the role of asymptomatic carriage in COVID-19 transmission. *eLife* **9**, 1–20 (2020).

[47] Han, E. *et al.* Lessons learnt from easing COVID-19 restrictions: an analysis of countries and regions in Asia Pacific and Europe. *The Lancet* **6736**, 1–10 (2020).

[48] Keeling, M. J. *et al.* Precautionary breaks planned limited duration circuit breaks to control the prevalence of COVID-19. Preprint at URL `https://medrxiv.org/cgi/content/short/2020.10.13.20211813` (2020).

[49] Kronbichler, A. *et al.* Asymptomatic patients as a source of COVID-19 infections: A systematic review and meta-analysis. *International Journal of Infectious Diseases* **98**, 180-186 (2020).

[50] Huang, L. *et al.* Rapid asymptomatic transmission of COVID-19 during the incubation period demonstrating strong infectivity in a cluster of youngsters aged 16-23 years outside Wuhan and characteristics of young patients with COVID-19: a prospective contact-tracing study. *Journal of Infection* **80**, e1-e13 (2020).

[51] Lavezzo, E. *et al.* Suppression of COVID-19 outbreak in the municipality of Vo, Italy. *Nature* **584**, 425–429 (2020).

[52] Chau, N. V. V. *et al.* The natural history and transmission potential of asymptomatic SARS-CoV-2 infection. *Clinical Infectious Diseases* **711** (2020).

[53] Aleta, A. *et al.* Modeling the impact of social distancing, testing, contact tracing and household quarantine on second-wave scenarios of the COVID-19 epidemic. Preprint at URL `https://doi.org/10.1101/2020.05.06.20092841` (2020).

[54] Chung, S.-C. *et al.* A rapid systematic review and case study on test, contact tracing, testing, and isolation policies for COVID-19 prevention and control. Preprint at URL `https://doi.org/10.1101/2020.06.04.20122614` (2020).

[55] Robert-Koch-Institut Epidemiologisches Bulletin 32/33 2020. URL `https://www.rki.de/DE/Content/Infekt/EpidBull/Archiv/2020/Ausgaben/32-33_20.pdf` (2020).

[56] Eddy, M. Welcome Back to Germany. Now Take Your Free Virus Test. *The New York Times* (2020).

[57] He, X. *et al.* Temporal dynamics in viral shedding and transmissibility of COVID-19. *Nature Medicine* **26**, 672–675 (2020).

[58] Kojaku, S., Hébert-Dufresne, L. & Ahn, Y.-Y. The effectiveness of backward contact tracing in networks. Preprint at URL `https://arxiv.org/abs/2005.02362v3` (2020).

[59] Smyrlaki, I. *et al.* Massive and rapid COVID-19 testing is feasible by extraction-free SARS-CoV-2 RT-qPCR. *Nature Communications* **11**, 4812 (2020).

[60] Cohen, A. & Kessel, B. False positives in reverse transcription PCR testing for SARS-CoV-2. Preprint at URL `https://doi.org/10.1101/2020.04.26.20080911` (2020).

[61] Cencetti, G. *et al.* Using real-world contact networks to quantify the effectiveness of digital contact tracing and isolation strategies for COVID-19 pandemic. Preprint at URL `https://doi.org/10.1101/2020.05.29.20115915` (2020).

[62] Kirkcaldy, R. D., King, B. A. & Brooks, J. T. COVID-19 and Postinfection Immunity: Limited Evidence, Many Remaining Questions. *JAMA* **323**, 2245-2246 (2020).

[63] an der Heiden, M. & Hamouda, O. Schätzung der aktuellen Entwicklung der SARS-CoV-2- Epidemie in Deutschland – Nowcasting. *Epidemiologisches Bulletin* **2020**, 10–15 (2020).

[64] Lauer, S. A. *et al.* The incubation period of coronavirus disease 2019 (COVID-19) from publicly reported confirmed cases: estimation and application. *Annals of internal medicine* **172**, 577-582 (2020).

[65] Shampine, L. F. & Reichelt, M. W. The MATLAB ode suite. *SIAM journal on scientific computing* **18**, 1–22 (1997).

[66] Contreras, S. *et al.* Statistically-based methodology for revealing real contagion trends and correcting delay-induced errors in the assessment of COVID-19 pandemic. *Chaos, Solitons & Fractals* **139**, 110087 (2020).

[67] Pan, A. *et al.* Association of public health interventions with the epidemiology of the COVID-19 outbreak in Wuhan, China. *JAMA* **323**, 1915–1923 (2020).

[68] Pan, F. *et al.* Time course of lung changes on chest CT during recovery from 2019 novel coronavirus (COVID-19) pneumonia. *Radiology* **295**, 715–721 (2020).

[69] Ling, Y. *et al.* Persistence and clearance of viral RNA in 2019 novel coronavirus disease rehabilitation patients. *Chinese medical journal* **133**, 1039–1043 (2020).

Acknowledgments

We thank the Priesemann group for exciting discussions and for their valuable comments. We also thank helpful comments and suggestions from Dr. Jakob Ruess (Inria), Prof. Dr. Ralf Meyer (Göttingen Uni), Prof. Dr. Álvaro Olivera-Nappa (Universidad de Chile). **Funding:** All authors received support from the Max-Planck-Society. SC acknowledges funding from the Centre for Biotechnology and Bioengineering - CeBiB (PIA project FB0001, Conicyt, Chile). ML, JD and PS acknowledge funding by SMARTSTART, the joint training program in computational neuroscience by the VolkswagenStiftung and the Bernstein Network. JZ received financial support from the Joachim Herz Stiftung. M. Wibral is employed at the Campus Institute for Dynamics of Biological Networks funded by the VolkswagenStiftung.

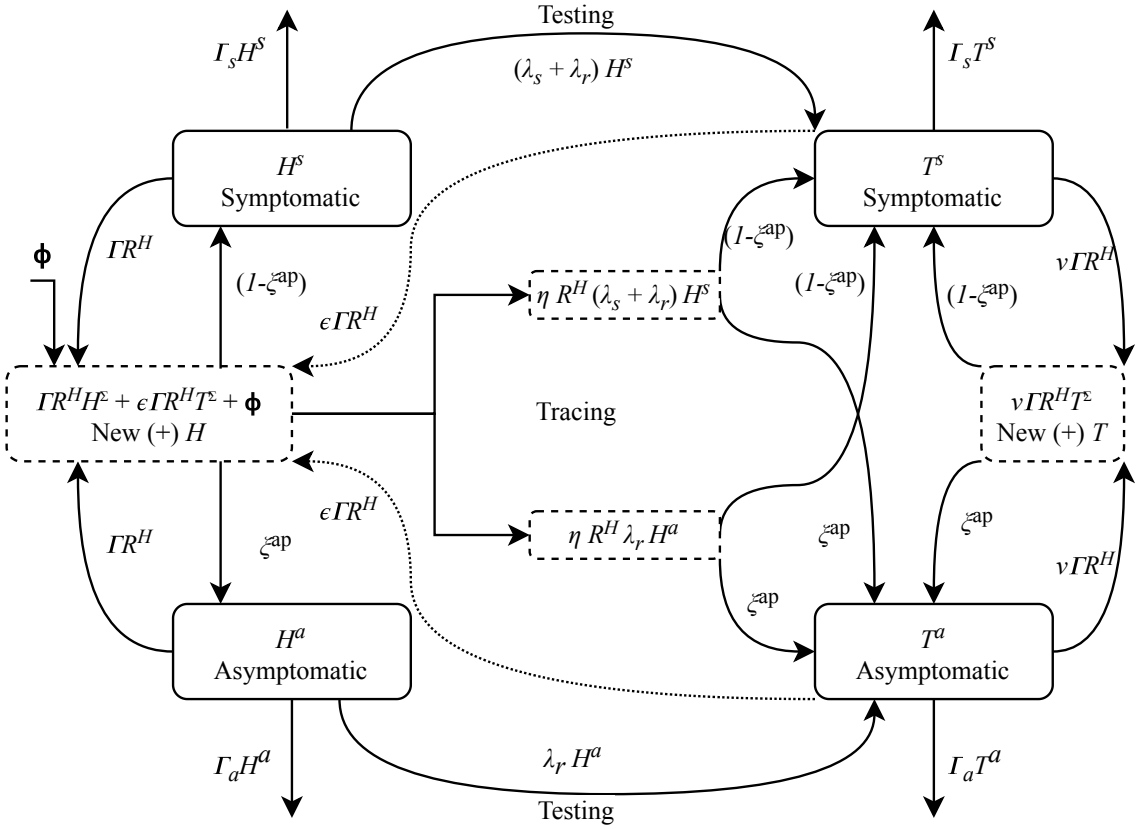
Author Contributions

SC, JD, JZ, VP designed research. SC conducted research. SC, JD, JZ, ML, M. Wibral, M. Wilczek, VP analyzed the data. SC, PS, ML, JU, SBM created figures. All authors wrote the paper.

Competing Interests

The authors declare no competing interests.

Supplementary Information: The challenges of containing SARS-CoV-2 via test-trace-and-isolate



Supplementary Figure 1: **Flowchart of the complete model.** This figure corresponds to Fig. 1 in the main manuscript.

Supplementary Note 1: Linear stability analysis

For analyzing the stability of the governing differential equations, namely, whether an outbreak could be controlled, we studied the linear stability of the system. The linearized system for equations (1)-(3) with limitless tracing capacity, is given by:

$$\frac{d}{dt}\begin{pmatrix} T \\ H \\ H^s \end{pmatrix} = \begin{pmatrix} \Gamma\left(\nu R_t^H - 1\right) & \lambda_r\left(\eta R_t^H + 1\right) & \lambda_s\left(1 + \eta R_t^H\right) \\ \Gamma\epsilon R_t^H & \Gamma\left(R_t^H - 1\right) - \lambda_r\left(1 + \eta R_t^H\right) & -\lambda_s\left(1 + \eta R_t^H\right) \\ (1-\xi^{\mathrm{ap}})\,\Gamma\epsilon R_t^H & (1-\xi^{\mathrm{ap}})\left(\Gamma R_t^H - \lambda_r\left(1 + \eta R_t^H\right)\right) & -\eta\,(1-\xi^{\mathrm{ap}})\,R_t^H\lambda_s - (\lambda_s + \lambda_r + \Gamma) \end{pmatrix}\begin{pmatrix} T \\ H \\ H^s \end{pmatrix} \tag{1}$$

By studying the eigenvalues of the associated matrix we can infer the stability of the solutions around the equilibrium. In particular, we define R^H_{crit} as the largest R_t^H such that the real part of $\mu_{\max}$, the largest eigenvalue of matrix A, is strictly negative.

Supplementary Note 2: Equilibrium equations for case numbers below tracing capacity

A system equilibrium is reached when time derivatives equals zero. That is by setting the left hand side in eqs. (1)-(3) of the main manuscript equal to zero, e.g., $dT/dt = 0$. Regarding the SIR-like model presented here, an equilibrium with non-zero new cases can be attained for a positive constant influx Φ and certain

combination of the parameters, and depending on whether the health authority's tracing capacity is exceeded or not. This equilibrium exhibits a stable number of daily new cases $\hat{N}^{\text{obs}} = N_{\infty}^{\text{obs}}$, which, excluding random testing ($\lambda_r = 0$), would take the form:

$$N_{\infty}^{\text{obs}} = \Gamma \nu R_t^H T_{\infty} + \lambda_s H_{\infty}^s + f(H^s, H), \tag{2}$$

where $f(H^s, H)$ is defined by equation (5) in the main manuscript. The convolution of reporting delays would not play a significant role (as cases would be constant).

For the case in which the tracing capacity is not exceeded ($\eta \lambda_s R_t^H H_{\infty}^s < n_{\max}$), and excluding random testing ($\lambda_r = 0$), setting equations eqs. (1)-(3) of the main manuscript equal to zero and expanding equation (2) gives the following set of equations:

$$T_{\infty} = \frac{\lambda_s \left(1 + \eta R_t^H\right)}{\Gamma \left(1 - \nu R_t^H\right)} H_{\infty}^s \tag{3}$$

$$H_{\infty} = H_{\infty}^s \frac{\lambda_s}{\Gamma} \left(\frac{\frac{\Gamma}{\lambda_s} + \xi^{\text{ap}}}{1 - \xi^{\text{ap}}} \right) \tag{4}$$

$$H_{\infty}^s = \frac{\Phi}{\lambda_s \left(1 + \eta R_t^H\right)} \left[\left(\frac{\epsilon R_t^H}{\nu R_t^H - 1} + R_t^H \right) - \left(R_t^H - 1\right) \frac{\eta R_t^H + \frac{1+\Gamma/\lambda_s}{1-\xi^{\text{ap}}}}{\eta R_t^H + 1} \right]^{-1} \tag{5}$$

$$N_{\infty}^{\text{obs}} = \Gamma \nu R_t^H T_{\infty} + \lambda_s H_{\infty}^s \left(1 + \eta R_t^H\right). \tag{6}$$

To calculate N_{∞}^{obs} in terms of the model's parameters, we insert equations (3)– (5) into equation (6):

$$N_{\infty}^{\text{obs}} = \lambda_s H_{\infty}^s \left(1 + \eta R_t^H\right) \left(\frac{1}{1 - \nu R_t^H} \cancel{-1+1} \right), \tag{7}$$

$$= \lambda_s H_{\infty}^s \frac{1 + \eta R_t^H}{1 - \nu R_t^H}. \tag{8}$$

This equilibrium is stable as soon as $R_t^H < R_{\text{crit}}^H$ (R_{crit}^H is calculated in Table 1).

To study the effect of Φ on the steady-state observed case numbers N_{∞}^{obs}, we evaluate the value of H_{∞}^s in equation 8 using equation 5:

$$\frac{\Phi \lambda_s \cancel{\left(1 + \eta R_t^H\right)}}{\left(1 - \nu R_t^H\right) \lambda_s \cancel{\left(1 + \eta R_t^H\right)}} \left[\left(\frac{\epsilon R_t^H}{\nu R_t^H - 1} + R_t^H \right) - \left(R_t^H - 1\right) \frac{\eta R_t^H + \frac{1+\Gamma/\lambda_s}{1-\xi^{\text{ap}}}}{\eta R_t^H + 1} \right]^{-1} = N_{\infty}^{\text{obs}}, \tag{9}$$

concluding that they are in direct proportionality, with a constant of proportionality k depending on the system's parameters:

$$\frac{N_{\infty}^{\text{obs}}}{\Phi} = k \left(\xi^{\text{ap}}, \lambda_s, \eta, \Gamma, \nu, \epsilon, R_t^H\right). \tag{10}$$

Equilibrium equations for case numbers above tracing capacity

We can also derive equilibrium equations for the case where tracing capacity is exceeded ($\eta \lambda_s R_t^H H_{\infty}^s > n_{\max}$). Remark that in this case, that critical reproduction number at which the equilibrium is stable, is smaller than for the $\eta \lambda_s R_t^H H_{\infty}^s < n_{\max}$ case.

When the tracing capacity is exceeded, the values returned by function $f(H^s, H)$ (defined by equation (5) in the main manuscript) are constant $f(H^s, H) = n_{\max}$. Then, setting the equations (1)-(3) of the main manuscript equal to zero leads to:

$$T_\infty = \frac{\lambda_s H^s_\infty + n_{\max}}{\Gamma\left(1 - \nu R^H_t\right)} \tag{11}$$

$$H_\infty = H^s_\infty \frac{\lambda_s}{\Gamma}\left(\frac{\frac{\Gamma}{\lambda_s} + \xi^{\text{ap}}}{1 - \xi^{\text{ap}}}\right) \tag{12}$$

$$\lambda_s H^s_\infty = \frac{n_{\max}\left(\frac{\epsilon R^H_t}{\nu R^H_t - 1} + 1\right) - \Phi}{\left(R^H_t - 1\right)\left(\frac{\frac{\Gamma}{\lambda_s} + \xi^{\text{ap}}}{1 - \xi^{\text{ap}}}\right) - \left(1 - \frac{\epsilon R^H_t}{1 - \nu R^H_t}\right)} \tag{13}$$

Similarly, we can derive an equation for $N_{\max}$, which represents the **maximum observed number of cases** at the tracing capacity limit, by using the new equilibrium values and the tracing-limit condition $f(H^s, H) = n_{\max}$ in equation (2):

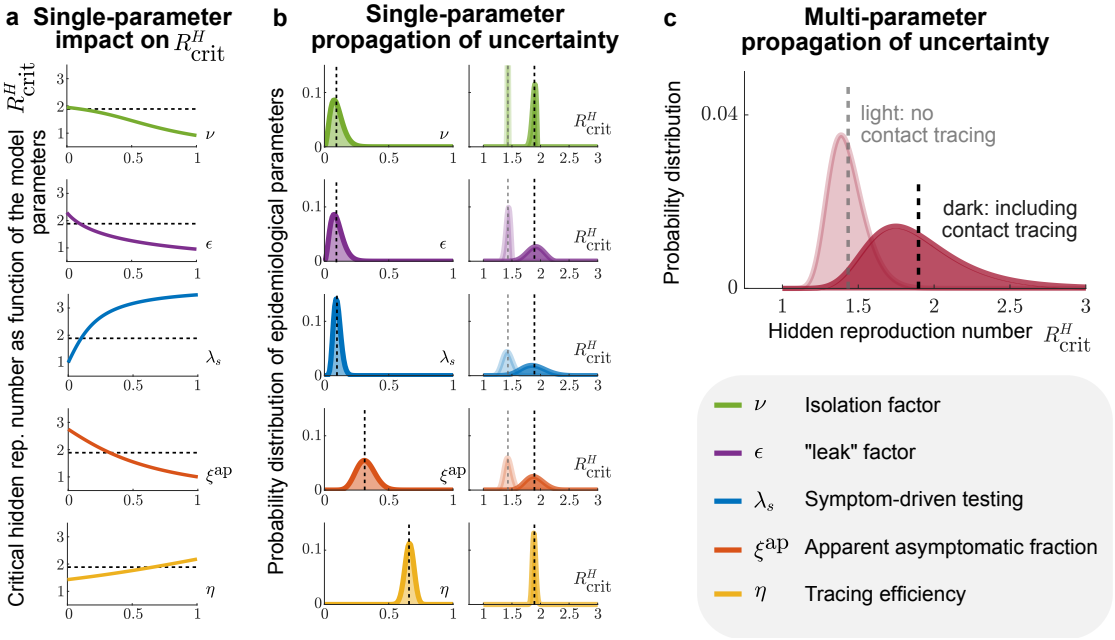
$$N^{\text{obs}}_\infty = \frac{\left(R^H_t - 1\right)\left(\frac{\frac{\Gamma}{\lambda_s} + \xi^{\text{ap}}}{1 - \xi^{\text{ap}}}\right) n_{\max} - \Phi}{\left(R^H_t - 1\right)\left(\frac{\frac{\Gamma}{\lambda_s} + \xi^{\text{ap}}}{1 - \xi^{\text{ap}}}\right) - \left(1 - \frac{\epsilon R^H_t}{1 - \nu R^H_t}\right)} \frac{1}{1 - \nu R^H_t} \stackrel{!}{=} N_{\max}. \tag{14}$$

Note that this approach to calculate $N_{\max}$ assumes the system is stable and has a finite equilibrium value. When the system is out of equilibrium, the value $N_{\max}$ is only an approximation for the number of observed cases at which tracing capacity is overwhelmed.

Supplementary Note 3: Parameter uncertainty propagation

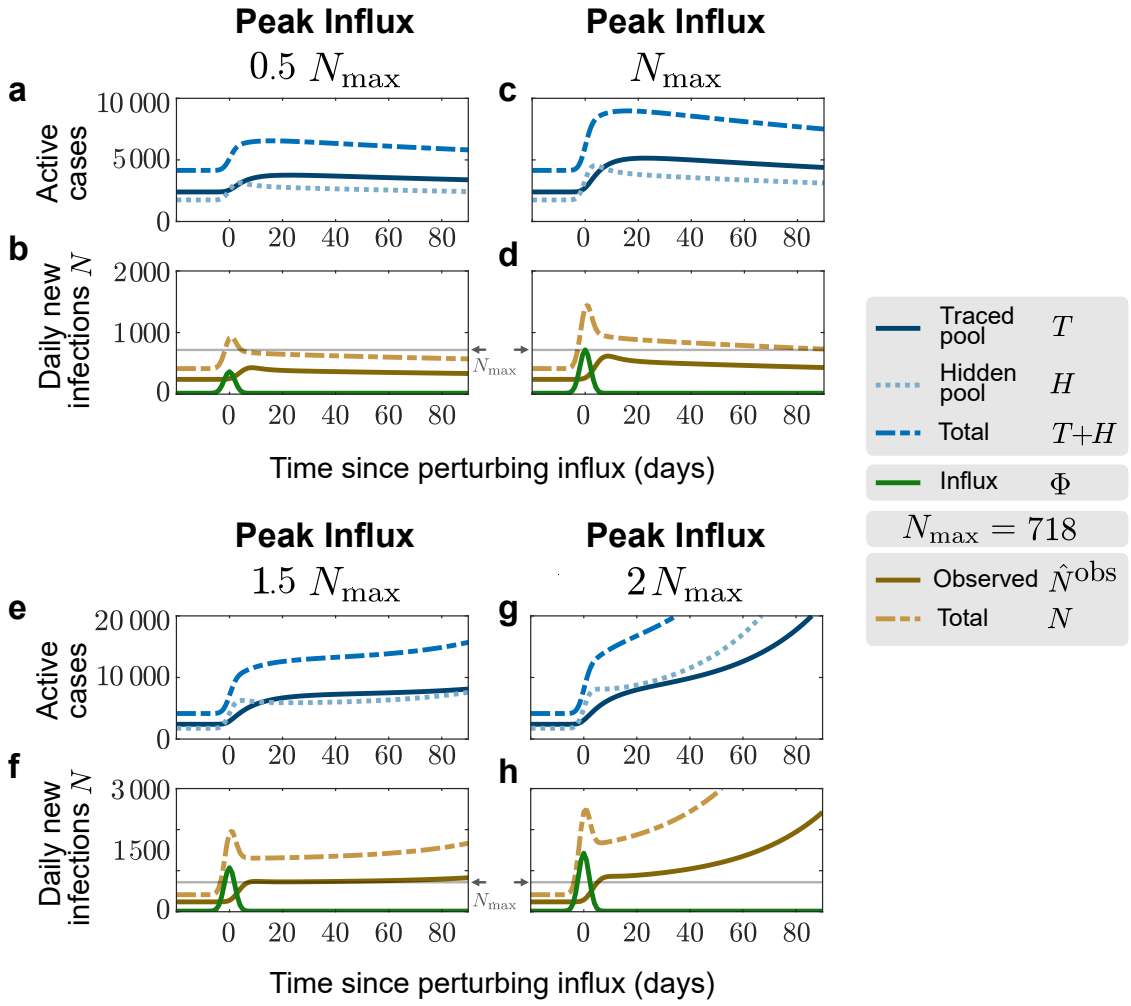
Supplementary Table 1: Parameter uncertainty propagation

Parameter	Meaning	Mean	95% CI	α	β	Dist.	Units
ξ^{ap}	Apparent Asymptomatic ratio	0.32	0.19–0.47	13.1	27.8	beta	–
λ_s	Symptom-driven test rate	0.10	0.05–0.16	10.7	96.3	beta	days^{-1}
ν	Isolation factor (traced)	0.10	0.03–0.22	3.5	31.5	beta	–
η	Tracing efficiency	0.66	0.59–0.73	117.9	60.7	beta	–
ϵ	Missed contacts (traced)	0.10	0.03–0.22	3.5	31.5	beta	–
$R^H_{\mathrm{crit}}\big\vert_{\eta=0.66}$	Critical reproduction number (hidden) (with $<\eta>=0.66$)	1.90	1.42–2.70	–	–	–	–
$R^H_{\mathrm{crit}}\big\vert_{\eta=0}$	Critical reproduction number (hidden) (with $\eta=0$)	1.42	1.23–1.69	–	–	–	–

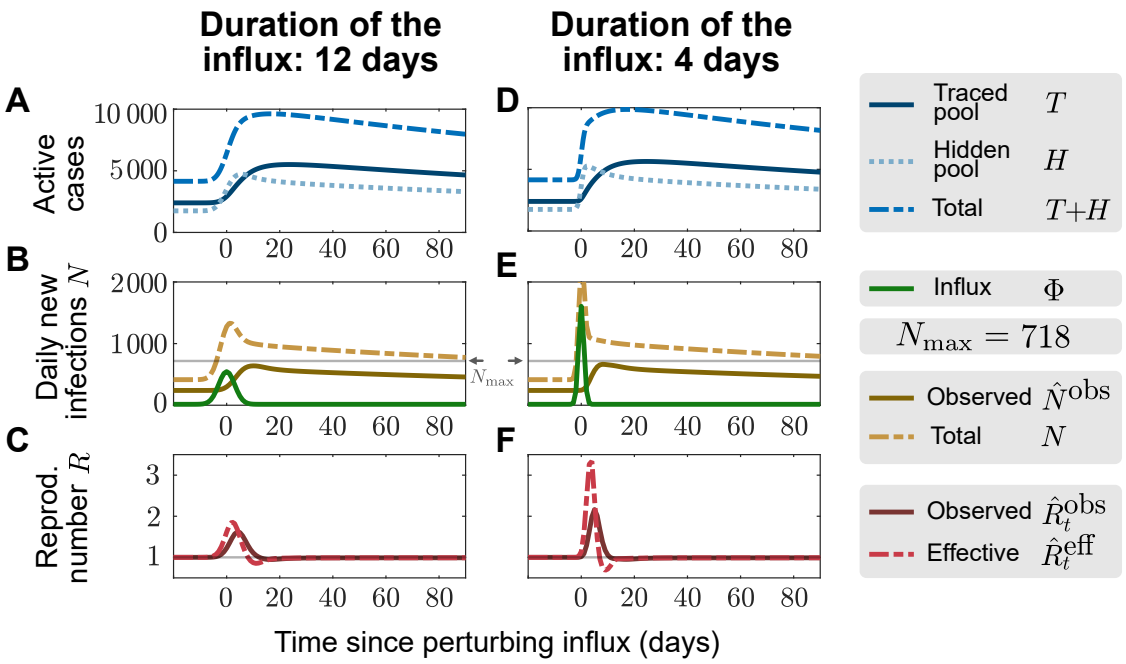


Supplementary Figure 2: **Propagation of TTI-parameter uncertainties to the critical reproduction number.** As the different parameters involved in our model play different roles, the way their variability propagates to R^H_{crit} differs, even when their variability profiles look similar. **(a)** Impact of single-parameter variation on the critical hidden reproduction number R^H_{crit}. To evaluate the monotony (direction) of their impact on R^H_{crit}, we scan their entire definition range, ignoring the practical feasibility of achieving such values. Dotted black line shows the default critical hidden reproduction number. **(b)** Univariate uncertainties of TTI parameters modelled by beta distributions centered on their default value (dotted black line), and the resulting distribution of critical reproduction numbers R^H_{crit} (right column). Results are shown assuming testing only (light colors) or testing and tracing (dark colors). The default value of R^H_{crit} is marked by the dotted lines, in the presence (black) or absence (grey) of tracing. **(c)** Distribution of critical reproduction numbers arising from multivariate uncertainty propagation given by the joint of the distributions shown in (a) for testing only (light colors), or testing and tracing (dark colors). The default value of R^H_{crit} is marked by the dotted lines, in the presence (black) or absence (grey) of tracing. Results show averages of 100 000 realizations.

Supplementary Note 4: Studying the effect of different influx scenarios on the TTI-conditional stability of the system



Supplementary Figure 3: **Effect of influx amplitude on the stability of the system.** This figure corresponds to Fig. 3 in the main text. For the default capacity scenario, we explore influxes of different amplitude: the peak of the influx is equal to 0.5 **(a,b)**, 1.0 **(c,d)**, 1.5 **(e,f)**, and 2 **(g,h)** times the -equilibrium- capacity limit of the health authorities $N_{\max}$. The influx is normally spread around day 0 with standard deviation $\sigma = 2$ days, corresponding to the 92 % of a total influx of, respectively, 1773, 3546, 5319, and 7092 individuals, entering the system over 7 days.



Supplementary Figure 4: **Effect of influx duration on the stability of the system.** This figure corresponds to Fig. 3 in the main text. For the default capacity scenario, we explore influxes of identical overall number spread over different time windows: 92 % of the 4000 infections enter the system in 12 days ($\sigma = 3$ days, **a-c**); or in 4 days ($\sigma = 1$ day,**d-f**).

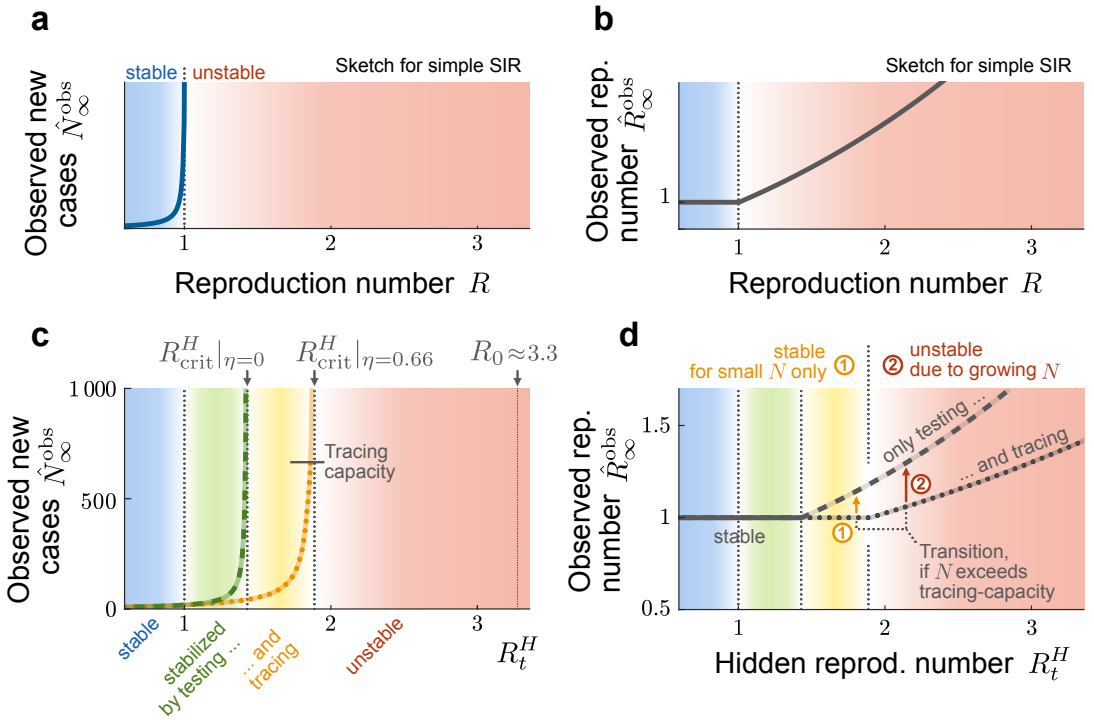
Supplementary Note 5: Testing and tracing give rise to two stabilized regimes of spreading dynamics

The simple SIR model with external influx exhibits two regimes: stable or growing: If the reproduction number R is less than one (blue region in Supplementary Fig. 5a.b), each new case infects less than one new case on average, and the number of new cases in equilibrium $\hat{N}_\infty^{\text{obs}}$ is finite (solid blue line in Supplementary Fig. 5a). If R is above one (red region in Supplementary Fig. 5a,b), each new case infects more than one new case, and the number of new cases grows quickly. These regimes are reflected in the equilibrium observed reproduction number $\hat{R}_\infty^{\text{obs}}$: In the stable regime, $\hat{R}_\infty^{\text{obs}} = 1$, and in the unstable regime $\hat{R}_\infty^{\text{obs}} > 1$ (solid black line in Supplementary Fig. 5b).

Distinct from the standard SIR model, our two-pool model with TTI exhibits two TTI-stabilized regimes of spreading dynamics: The first regime requires only to isolate persons with positive test results ("testing-stabilized"), the second requires in addition to find and isolate contacts of a positively tested person ("tracing-stabilized", Supplementary Fig. 5c,d). Due to the stabilization, the transition to instability for these two regimes is shifted towards hidden reproduction numbers R_t^H above one (dotted grey lines in Supplementary Fig. 5c). As in the classical stable regime, the number of new cases in equilibrium $\hat{N}_\infty^{\text{obs}}$ diverges when approaching these critical points (dashed green and dotted orange lines in Supplementary Fig. 5c). The ultimately unstable regime begins at $R_t^H = R_{\text{crit}}^H \simeq 1.9$ for our default parameters. Note that R_{crit}^H is below the basic reproduction number reported for SARS-CoV-2 ($R_0 \approx 3.3$ [1–3]), however, it may already be attained by reducing contacts by 40 % from levels at the beginning of the pandemic.

Supplementary Note 6: A limited tracing capacity renders the tracing-stabilized regime meta-stable.

The amount of contacts that can reliably be traced by health authorities is limited due to the work to be performed by trained personnel: Contact persons have to be identified, informed, and ideally also counseled during the preventive quarantine. Exceeding the tracing capacity limit destabilizes an otherwise stable regime, rendering it effectively meta-stable (amber in Supplementary Fig. 5c,d. Once the tracing capacity is exceeded,



Supplementary Figure 5: **Testing and tracing give rise to two TTI-stabilized regimes of spreading dynamics.** This figure is a more detailed version of Fig. 5 in the main text. In the simple SIR model with external influx **(a,f)**, the spreading dynamics exhibit a stable and an unstable regime (blue and red regions, respectively). In addition to these, our two-pool model exhibits **(c,d)** two "TTI-stabilized" regimes that arise from the isolation of infected persons upon testing positive (green region) or upon being traced as a contact of an infected person (amber region). **(a)** Observed case numbers $\hat{N}_\infty^{\text{obs}}$ in the simple SIR model with external influx approach a finite equilibrium in the stable regime (solid blue line). As the reproduction number R approaches the critical point at $R = 1$, the case numbers in equilibrium $\hat{N}_\infty^{\text{obs}}$ diverge, growing uncontrolled in the unstable regime. **(b)** The asymptotic observed reproduction number $\hat{R}_\infty^{\text{obs}}$ inferred from the observed new cases $\hat{N}_\infty^{\text{obs}}$ in the simple SIR model with external influx is always 1 in the stable regime, but reflects the true value R in the unstable regime (solid grey line). **(c)** Daily number of new infections $\hat{N}_\infty^{\text{obs}}$ in our two-pool model are finite in the stable and stabilized regimes, but diverge upon approaching the critical points of the "testing only" or "testing and tracing" strategies (dashed green and dotted orange lines, respectively). They are infinite in the unstable regime, or when the tracing capacity limit is reached (black bar). The exact position of the critical points of the stabilized regimes depend on the efficiencies of the respective strategies: Symptom-driven testing alone ($\eta = 0$, green) can only stabilize the spread for $\hat{R}_\infty^{\text{obs}} < R^H_{\text{crit}}|_{\eta=0} \approx 1.5$, while symptom-driven testing and tracing ($\eta = 0.66$, amber) can stabilize the spread for up to $R_t^H < R^H_{\text{crit}}|_{\eta=0.66} \approx 1.9$ for our default parameters (Table. 1). **(d)** The observed reproduction number $\hat{R}_\infty^{\text{obs}}$ of a system stabilized by symptom-driven testing and tracing is always 1 in the "stable" and "testing-stabilized" regimes (solid grey line). In the meta-stable "testing-and-tracing-stabilized" regime (dotted grey line), $\hat{R}_\infty^{\text{obs}} = 1$ as long as the tracing capacity is not exceeded. If exceeded, the system behaves asymptotically as if there was only symptom-driven testing in place (transition 1, see also Fig. 3), which can only slow down, but not control the spread anymore. In the "unstable" regime, the observed reproduction number $\hat{R}_\infty^{\text{obs}}$ always increases with R_t^H – thus, the number of cases always grows. As long as the tracing capacity is not exceeded by this growth, testing-and-tracing slows down the spread (dotted grey line) – afterwards the system behaves asymptotically as if there was only symptom-driven testing slowing down the spread (transition 2, see also Fig. 6). The curves showing observed new cases are obtained from the analytical description of the equilibrium for unlimited tracing capacity (equations (3) - (5)). The curves showing the observed reproduction number are obtained from the linear stability analysis (equation (1)).

the system will behave asymptotically as if it had testing only, i.e. the effective and observed reproduction number will strongly increase (transition 1) from dotted to dashed grey line in Supplementary Fig. 5d).

This demonstrates that a low number of new infections is essential to control the spread when $R_t^H > 1$. Crossing the capacity limit of tracing, $N_{\max}$, leads to a self-accelerating spread, and thereby presents

a qualitatively new tipping point to instability in an otherwise stable system. - rendering it effectively meta-stable.

The transition from the meta-stable regime to the unstable regime happens when the tracing system is overwhelmed due to the number of observed new cases exceeding the tracing capacity ($\hat{N}^{\text{obs}} > N_{\text{max}}$). This can occur because of an increased influx Φ of infected people, e.g. returning from holiday, or a super-spreading event.

Supplementary Note 7: Incorporating different transmissibility of asymptomatic and symptomatic cases.

In the main text, we assumed that hidden asymptomatic and symptomatic infections would spread with identical reproduction number R_t^H. In reality, asymptomatic cases tend to have a lower viral load, but might have more contacts than hidden symptomatic cases because they do not decrease their movement after falling sick. Consequently, asymptomatic infections could spread with lower or higher reproduction number reproduction number than symptomatic cases.

We can model this difference in reproduction number by introducing an effective relative transmissibility factor χ: $R_t^{H,a} = \chi R_t^{H,s}$. The exact value of this factor is a function of the viral load, the infection time and the number of contacts, which we all do not model explicitly. Additionally, our model treats *real* and *apparent* asymptomatic cases (those that do net get tested) in the same manner, which should also be noted when interpreting the exact value of χ. Incorporating all of these influences into a single effective factor allows us to study how the relative transmissibility of *apparent* asymptomatic cases impacts the stability of the system.

Regardless of the relative transmissibility of asymptomatic and symptomatic cases, the overall reproduction number R_t^H can be inferred from the average spread in the population. It therefore must stay the same for all values of χ, which can be achieved by rescaling the transmissibility of symptomatic cases appropriately. The correct rescaling can be found from the following equation which relates the reproduction numbers in an equilibrium state where asymptomatic carriers occupy a fraction ξ^{ap} of the total infections:

$$R_t^H = R_t^{H,a}\xi^{\mathrm{ap}} + R_t^{H,s}\left(1-\xi^{\mathrm{ap}}\right). \tag{15}$$

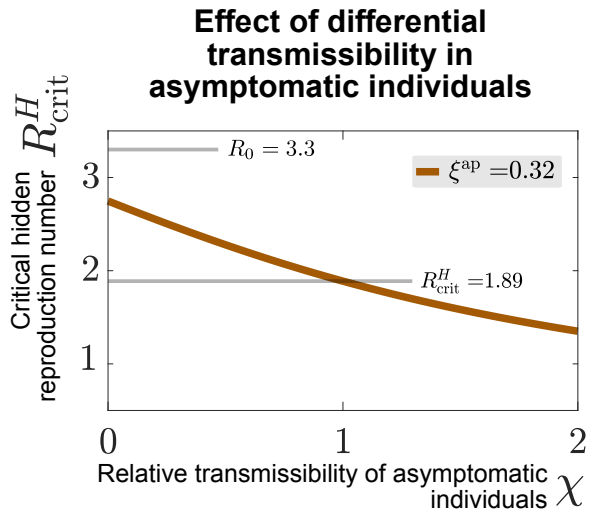
Combining this equation with that describing the relative transmissibility ($R_t^{H,a} = \chi R_t^H$) gives an expression for the rescaled transmissibility of symptomatic infections:

$$R_t^{H,s} = \underbrace{\left(\frac{1-\chi\xi^{\mathrm{ap}}}{1-\xi^{\mathrm{ap}}}\right)}_{\chi^s} R_t^H. \tag{16}$$

To analyze the stability of this system, we need to write detailed equations for all the compartments, as schematized in 1. After linearizing the system in the shape $x' = Ax$, where $x = (T^s, T^a, H^s, H^a)$ and A is given by equation 17, we study its eigenvalues. Critical values of the reproduction number R_{crit}^H are presented in Supplementary Fig. 6.

$$A = \begin{pmatrix} \xi^s\nu R_t^H\Gamma\chi^s-\Gamma & \xi^s\nu R_t^H\Gamma\chi & (\lambda_r+\lambda_s)(1+\xi^s\eta R_t^H\chi^s) & \xi^s R_t^H\eta\lambda_r\chi \\ \xi\nu R_t^H\chi^s\Gamma & \xi\nu R_t^H\Gamma\chi-\Gamma & (\lambda_r+\lambda_s)\eta R_t^H\xi\chi^s & \xi R_t^H\eta\lambda_r\chi+\lambda_r \\ \xi^s\epsilon R_t^H\Gamma\chi^s & \xi^s\epsilon R_t^H\Gamma\chi & -(\lambda_r+\lambda_s)(1+\xi^s\eta R_t^H\chi^s)-\Gamma+\xi^s R_t^H\Gamma\chi^s & -\xi^s R_t^H\eta\lambda_r\chi+\xi^s R_t^H\Gamma\chi \\ \xi\epsilon R_t^H\Gamma\chi^s & \xi\epsilon R_t^H\Gamma\chi & -\xi\eta R_t^H(\lambda_r+\lambda_s)\chi^s+\xi R_t^H\Gamma\chi^s & -\lambda_r-\xi R_t^H\eta\lambda_r\chi+\xi R_t^H\Gamma\chi-\Gamma \end{pmatrix} \tag{17}$$

where $\xi^s = 1-\xi$ and $\chi^s = (1-\chi\xi)/\xi^s$



Supplementary Figure 6: **Effect of differential transmissibility of asymptomatic and symptomatic infections on the critical reproduction number.** This figure is similar to those in Supplementary Fig. 2A, but explores the impact of an additional parameter: the relative transmissibility factor χ accounts for the fact that asymptomatic individuals might be less ($\chi < 1$) or more ($\chi > 1$) infectious than symptomatic individuals. Solid brown curve shows the critical reproduction number computed from linear stability analysis (equation 17). Dashed lines show the default value for $\chi = 1$ and the basic reproduction number R_0, respectively.

Supplementary References

[1] Liu, Y., Gayle, A. A., Wilder-Smith, A. & Rocklöv, J. The reproductive number of COVID-19 is higher compared to SARS coronavirus. *Journal of travel medicine* **27**, taaa021 (2020).

[2] Alimohamadi, Y. *et al.* Estimate of the Basic Reproduction Number for COVID-19: A Systematic Review and Meta-analysis. *J Prev Med Public Health* **53**, 151–157 (2020).

[3] Barber, A. *et al.* The basic reproduction number of SARS-CoV-2: a scoping review of available evidence. Preprint at URL `https://doi.org/10.1101/2020.07.28.20163535` (2020).